BRECCIA OF FROG LAKES: RECONSTRUCTING TRIASSIC VOLCANISM AND SUBDUCTION INITIATION IN THE EAST-CENTRAL SIERRA NEVADA, CALIFORNIA

Sarah Elizabeth Roberts

Submitted to the faculty of the University Graduate School
in partial fulfillment of the requirements
for the degree of
Master of Science
in the Department of Earth Sciences,
Indiana University
July 2013

Accepted by the Faculty of Indiana University, in partial fulfillment of the requirements for the degree of Master of Science.

_____

Andrew P. Barth PhD, Chair

_____

Gary D. Rosenberg PhD

Master's Thesis
Committee

_____

Gabe M. Filippelli PhD

ACKNOWLEDGMENTS

Andy Barth, Gabe Filippelli, Gary Rosenberg,

Joe Wooden, Nancy Riggs, Rita Economos,

Rosalice Buhrer, and Clive Neal.

ABSTRACT

Sarah Elizabeth Roberts

BRECCIA OF FROG LAKES: RECONSTRUCTING TRIASSIC VOLCANISM AND SUBDUCTION INITIATION IN THE EAST-CENTRAL SIERRA NEVADA, CALIFORNIA

The Antler and Sonoma orogenies occurred along the southwest-trending passive Pacific margin of North America during the Paleozoic concluding with the accretion of the McCloud Arc. A southeast-trending sinistral transform fault truncated the continental margin in the Permian, becoming a locus for initiation of an east-dipping subduction zone creating the Sierran magmatic arc. Constrained in age between two early Triassic tuff layers, the volcanic clasts in the breccia of Frog Lakes represent one of the earliest records of mafic magmatism in the eastern Sierra Nevada. Tholeiitic rock clasts found in the breccia of Frog Lakes in the Saddlebag Lake pendant in the east central Sierra Nevada range in composition from 48% to 63% SiO2. Boninites produced by early volcanism of subduction initiation by spontaneous nucleation at the Izu-Bonin-Mariana arc are more depleted in trace element concentrations than the clasts while andesites from the northern volcanic zone of the Andes produced on crust 50 km thick have similar levels of enrichment and provide a better geochemical modern analogue. Textural analysis of the breccia of Frog Lakes suggest a subaqueous environment of deposition from a mature magmatic arc built on continental crust > 50 km thick during the Triassic. The monzodiorites of Saddlebag and Odell Lakes are temporal intrusive equivalents of the breccia of Frog Lakes and zircon geochemistry indicates a magmatic arc petrogenesis.

Andrew P. Barth PhD, Chair

TABLE OF CONTENTS

Introduction

Mafic rock clasts found in the breccia of Frog Lakes (BFL) represent one of the earliest records of Mesozoic mafic magmatism in the Sierra Nevada and provide insight as to the petrology of mafic magmatism during subduction initiation beneath the east Sierran arc. Because the BFL is constrained stratigraphically between the Saddlebag and Greenstone Lake ash-flow tuffs, the depositional age for the BFL and the associated tuffs also provide a well-constrained record of the timing of subduction initiation. In this study, the timing of initiation of Mesozoic magmatism is determined through zircon geochronology of these overlying and underlying ash-flow tuff units. The whole rock major and trace element geochemistry of the breccia clasts is compared to volcanic rocks erupted in modern oceanic island arcs and continental island arcs, indicating the structural setting of the east Sierran arc, the thickness of the underlying arc crust, and the evolutionary stage of the arc during the Late Triassic.

The BFL correlates temporally with intrusive rocks of the monzodiorites of Odell and Saddlebag Lakes, and the intrusive bodies potentially represent the intrusive equivalents of these volcanic rocks. In this study, I argue that zircon age and geochemistry can be used to identify the petrogenetic setting of the intrusive rocks and to identify the monzodiorites as the intrusive equivalents of the clasts in the BFL.

Geologic Setting of Arc Initiation in the Western U.S.

The evolution of the western margin of North America in California was characterized by a change in tectonic regimes from a passive margin with continent-derived sedimentation in the Paleozoic to active subduction in the Mesozoic. The contrasting depositional and tectonic settings represented by upper Paleozoic and lower Mesozoic rocks of the western U.S Cordillera offer a sedimentary record of the events that affected the continental margin (Miller et al., 1992). A region of poorly understood paleogeography of offshore basins and volcanic island arcs lay to the west of the Paleozoic continental shelf. Crustal shortening and consequent deformation affected offshore basins and the edge of the southwest-trending continental shelf twice, resulting in the thrust emplacement of basinal rocks onto the continental shelf as the Roberts Mountains and Golconda allochthons during the Antler and Sonoma orogenies, respectively. In the westernmost part of the Cordillera, two contrasting but parallel belts of Upper Paleozoic rocks are present, the eastern belt consisting of continuous sequences of Devonian to Jurassic volcanic and sedimentary strata deposited in an island arc setting and the western containing allochthonous masses of Paleozoic limestone, chert, and mafic volcanic rocks thought to have been accreted in a subduction zone setting. The southwest-trending continental margin was truncated and a southeast-trending, east-dipping subduction zone is inferred to have been established by at least the Late Permian as dated by the calc-alkaline magmatism in the adjacent arc (Miller et al., 1992). Today, these two belts are represented by scattered exposures in the northern Sierra Nevada, Klamath Mountains, northwestern Nevada, Oregon, and Washington. Based on the geologic history, tectonic setting, and faunal evidence, the two belts are believed to have constituted an island arc system and a subduction zone complex that consumed intervening oceanic lithosphere and collided during the Late Jurassic Nevadan orogeny (Schweickert and Cowan, 1975).

The Antler and Sonoma orogenies were the first to occur on the Pacific margin as it had been left a passive margin following Precambrian rifting (Nilsen and Stewart, 1980). Allochthons of ocean strata were thrust eastward across the seaward flank of

the southwest-trending miogeoclinal belt during the Late Devonian to the Early Triassic (Dickinson, 2004). For the allochthons to have been thrust eastward, the margin of the Laurentian continent and offshore oceanic crust of marginal seas were being drawn westward into the subduction zones of intraoceanic island arcs.

The Antler orogeny spanned from the Devonian to the Mississippian and is recorded by the emplacement of the Roberts Mountains allochthon. Preceding the orogeny, western North America was an Atlantic-type continental margin. Miogeoclinal shelf deposits of carbonate, shale, and quartzite were deposited to the east while deep marine eugeoclinal chert, argillite, greenstone, and quartzite were deposited to the west (Nilsen and Stewart, 1980). The Antler orogeny was the first deformation event to significantly alter patterns of shelf sedimentation in western North America during the Paleozoic and involved the deformation of the outer edge of the continental shelf during the eastward thrust emplacement of basinal-facies rocks of the Roberts Mountains allochthon (Miller et al., 1992). The Roberts Mountains allochthon consists of deformed Upper Cambrian to Devonian chert, argillite, sandstone, and greenstone (Miller et al., 1992). The easternmost sections of the allochthon are exposed in Nevada, and the eastern limit of the allochthon can be inferred by the exposures in Nevada. As it exists currently with an overlap of Devonian autochthonous shelf strata, the allochthon traveled a distance of 140 km, although this amount may be skewed by later Basin and Range extension. Some exposures of these allochthonous rocks occur in the eastern Sierra Nevada, including the northern Ritter Range pendant and the Saddlebag Lake pendant (Greene et al., 1997; Schweickert and Lahren, 1987).

During the Late Permian and/or Early Triassic, the allochthonous Havallah sequence was transported along the Golconda thrust over autochthonous shallow-marine and nonmarine assemblages and older rocks of the Roberts Mountains allochthon during the Sonoma orogeny. The Golconda allochthon extends from northern Nevada to the eastern Sierra Nevada and the southern extent of the allochthon is unknown. Rocks found within the allochthon range in age from latest Devonian to Late Permian and are mostly composed of sedimentary rocks and lesser

greenstone (Miller et al., 1992). Widespread Permian volcaniclastic strata in the Golconda allochthon, including andesitic arc-derived debris along with coarse volcanogenic debris flows containing boulders and cobbles of plutonic rocks dated as 267 Ma, indicate the encroachment or establishment of a volcanic arc system, the McCloud Arc, west of the continental shelf (Miller et al., 1992). After the accretion of the McCloud Arc along a southwest-trending passive margin during the Sonoma orogeny, a southeast-trending sinistral transform fault truncated the edge of the continental margin (Stones and Stevens, 1988). A Pennsylvanian to Permian carbonate shelf traces the southeastward truncated continental margin. By the Permian, this newly truncated margin became the locus for the initiation of an east-dipping subduction zone and the creation of the east Sierran magmatic arc.

Stratigraphic Setting of Volcanic Rocks in the Saddlebag Lake Pendant

The evolution of the continental margin during the early Mesozoic is recorded in the stratigraphy of the Saddlebag Lake pendant (Figure 1). Located in the east-central Sierra Nevada, Paleozoic and Mesozoic sedimentary and extrusive volcanic rocks of the pendant record the change from the sedimentation associated with the Antler and Sonoma orogenies to the inception of subduction and arc magmatism along the sialic continental margin (Barth et al., 2011). Virginia Lakes is located in the eastern edge of the Saddlebag Lake pendant. Paleozoic and Mesozoic rocks of the Saddlebag Lake pendent are repeated three times by thrust faults. The Saddlebag Lake locality is built on the Permian Diablo and Ordovician Palmetto formations representing the Sonoma and Antler orogenies respectively (Figure 2). The Virginia Lakes locality is built on the Triassic Candelaria Formation, representing the Sonoma orogeny (Schweickert and Lahren, 1987). The Candelaria Formation is a quartzofeldspathic siltstone and sandstone with chert and shale lithic grains. Overlying the Candelaria is the pumice-poor ash flow tuff of Black Mountain containing phenocrysts of feldspar and quartz (Barth et al., 2011). The last vestige of continental sedimentation is found in the overlying conglomerate of Cooney Lake containing clasts of quartzite, chert, and argillite with an ash matrix (Riggs, pers. comm., 2012). Overlying the conglomerate of Cooney Lake is the tuff of Saddlebag Lake. Barth et al. (2011) describes the tuff of Saddlebag Lake is a very light tan to light grey ash-flow tuff with dark grey flattened pumice fiamme up to 15 cm long, and 5 to 10% phenocrysts of a mafic mineral (possibly both amphibole and biotite), feldspar and quartz. The mafic phenocrysts are entirely recrystallized, but appear to have been mostly subhedral to euhedral amphibole up to about 1 mm across. Feldspar phenocrysts are broken, anhedral crystals up to 3 mm in long dimension, and are typically partially to completely replaced by epidote + calcite. Quartz phenocrysts up to 4 mm across are rarely euhedral, but more commonly are rounded, broken and locally deeply embayed.

U/Pb geochronology of the tuff of Saddlebag Lake performed by Barth et al. (2011) at Sawmill Canyon yielded an age of 224 ± 1 Ma, and at Virginia Lakes the tuff yielded an age of 223 ± 2 Ma (Douglas et al., 2010).

The uppermost part of the tuff of Saddlebag Lake, approaching the contact with the overlying unit, the BFL, consists of fine-grained, laminated sedimentary successions that can be divided into five distinct transitional units (Figure 3). The base of the first transitional tuff unit features reverse coarsening with poorly-sorted lithic fragments up to 5mm long and ½ mm laminae. A gradational contact leads to normal grading with larger (up to 20mm) lithic clasts. Thin laminae again define a gradational contact to a normally-graded bed that shows evidence of broad, shallow and erosive channeling (Figures 4 and 5). The base of the second transitional tuff unit has large phenocrysts of quartz and feldspar and cuts down into the first transitional tuff unit (Figures 6 and 7). Overall the composition of second transitional tuff unit is less than 5 % quartz and 2% feldspar. Fine-grained dark laminae 2-15 cm apart progressively become thinner and more discontinuous laminae up section until they become undulatory. The third transitional tuff unit has an undulatory base with continuous laminae 4-6 cm thick producing alternating banding with no grading (Figure 8). More abundant plagioclase is found in the third transitional tuff unit with 15% subhedral plagioclase 1-3 mm long and 5% quartz 0.5mm wide.

The bottom half of fourth transitional tuff unit is homogenous with 7 % quartz phenocrysts measuring 0.5-1 mm long, 5% plagioclase phenocrysts 1-3mm long, and large (up to 10 cm) lithic clasts (Figures 9 and 10). The upper half of the unit has alternating coarse (7-15 cm thick) and fine (1.5 cm thick) layers, the coarse layers containing 20% subhedral plagioclase ranging in length from 0.5-2mm, 7% subhedral quartz 0.5-1mm long and 2% epidote and mafic minerals. The fifth transitional tuff unit is texturally homogenous unit with no laminae or depositional features containing 5-30 cm mafic to felsic poorly sorted clasts and lithic fragments (Figure 11). Composition is 10% quartz phenocrysts, 15% plagioclase and 3% mafic minerals.

The BFL contains predominantly angular and non-juvenile clasts of basalt, andesitic basalt, and andesite. The mafic breccia is a laterally extensive, mostly massive and very poorly sorted, matrix supported tuff breccia, with up to 60% clasts. The most common rock type in the Virginia Lakes section is a matrix supported breccia composed of angular to subrounded clasts up to ~0.5 m. Quartzite and other sedimentary clasts are rare (Figure 12). A less common rock type comprises mixed-clast breccias with both angular clasts and clasts with highly irregular, fluidal borders with the matrix (Figure 13). Light microscope images of mafic rock clasts showing altered and recrystallized porphyritic texture due to metasomatism or metamorphism. Large euhedral to subhedral plagioclase phenocrysts altered to epidote and hornblende phenocrysts altered to chlorite suggest a greenschist or epidote hornfels facies (Figures 14 and 15). Some preservation of the original matrix is also observed. Calcite is seen replacing phenocrysts in some of the samples suggesting fluid and alkali transfer (Figure 16).

Overlying the BFL is the tuff of Greenstone Lake. Barth et al. (2011) describes the tuff as a tan to medium grey and usually relatively pumice-poor ash-flow tuff with dark grey flattened pumice fiamme up to 5 cm long, and about 10% phenocrysts of a recrystallized mafic mineral, feldspar and quartz (Figure 17). Phenocrysts of both plagioclase and alkali feldspar are anhedral, broken crystals up to 2 mm in long dimension. The most abundant phenocrysts are quartz crystals up to 3 mm across that are rarely euhedral, but most commonly rounded, broken and locally deeply embayed. Barth et al. (2011) reported a U/Pb age of 219 ± 1 Ma for the tuff of Greenstone Lake at Sawmill Canyon, and the tuff of Greenstone Lake at Virginia Lakes yielded an age of 220 ± 2 Ma (Douglas et al., 2010).

Geologic Setting of Intrusive Rocks

The monzodiorites of Odell and Saddlebag Lakes represent the potential intrusive equivalents of the BFL. Located south of Virginia Lakes, the monzodiorites are exposed around Odell and Saddlebag Lakes in southern Saddlebag Lake pendant (Figure 1), where they intrude Paleozoic metasedimentary rocks (Bateman et al., 1983; Schweickert and Lahren, 1999). U/Pb dating of zircons from the monzodiorite at Odell Lake performed by Barth et al. (2011) has shown the pluton to be 221 ± 2 Ma, and a statistically identical age of 220 ± 2 Ma was measured for the monzodiorite at Saddlebag Lake (Barth et al., unpublished data). The emplacement of these plutons corresponds temporally to the depositional age of the BFL as constrained by the ages of the tuffs of Greenstone Lake and Saddlebag Lake (Figure 2).

Samples and Analytical Methods

Nine rock clasts from the BFL (BFL) were crushed with a sledge hammer followed by a jaw crusher and powdered in a WC-lined mixer mill. Whole rock major and trace element geochemistry was analyzed at Michigan State University. Major elements along with Rb, Sr, and Zr were measured using X-ray fluorescence (XRF) and trace elements were analyzed by inductively coupled plasma-mass spectrometer (ICP-MS) (Table 2). In-run precision was monitored using JB-1a basalt and JA3 andesite rock standards, and is better than 1% for most major elements and trace elements present in abundances >100 ppm analyzed by XRF, and 2-5% for trace elements analyzed by ICP-MS. CO_2% and H_2O% was measured using Carbon Hydrogen Nitrogen Sulfur analysis by Flash EA 1112 Elemental Analyzer at IUPUI. 2,5-(Bis(5-tert-butyl-2-benzo-oxazol-2-yl) thiophene (BBOT) standard was also measured in triplicate to produce a precision of better than 0.5%.

Uranium and lead isotopes and trace element abundances in zircons were measured using the U.S. Geological Survey sensitive high-resolution ion microprobe (SHRIMP) at Stanford University. The SHRIMP was built with geological applications in mind and incorporates a very large mass analyzer to achieve a high mass resolution while also eliminating most major isobaric interferences (Ireland, 1995). To separate the zircons from the monzodiorites, samples were placed in a jaw crusher followed by a disc mill to obtain sand-sized grains. After washing to remove fine rock powder, samples were sieved to separate grains 250 to 50 μm in size. Magnetite was removed using a strong hand magnet and the remaining sample was put through a Frantz magnetic separator set at 1.5 amperes and a side-slope angle of 20 degrees from horizontal and 15 degree down-slope tilt. Zircons were separated from the remaining non-magnetic fraction using Methylene Iodide (density of 3.3 g/cm^3), allowing zircon crystals of 4.6 g/cm^3 to sink and segregate themselves from the remaining lighter minerals. Zircons were selected from the remaining grains and mounted in epoxy along with reference zircons. The mount was polished, cleaned, and coated with gold. Scanning electron microscope (SEM) cathodoluminescence (CL) images of the zircons

show oscillatory zoning in euhedral to subhedral zircon grains ranging in size from 75 µm to 225 µm long (Figure 18). Primary ion beam diameter of 25 µm along with a sputtering rate of 1 nm/s for 16 minutes results in a primary analytical volume of approximately 490 μm^3. Based on intermittent analyses of the standard, Ce and Hf show a precision of better than 3%; Sm, Gd, Dy, Er, and Th have a precision of better than 4%; Y, Nd, Eu, Yb, and U have precisions ranging from 4 to 6.1%; La shows the poorest precision at 14.9%.

Results

Whole Rock Geochemistry of Breccia Clasts

Whole rock major element and trace element geochemistry was completed on nine rock clasts from the BFL for this study (Table 1). Petrographic examination of the clasts shows alteration to a low-grade, greenschist facies assemblage, as seen in Figures 14-16. With alteration being suspected among the clasts, whole rock geochemical results were treated with caution, as alkali content of the clasts could be altered. For example, development of calcite as shown in Figure 16 could indicate enriched Ca concentrations relative to initial formation of the clast. As the degree of alteration varied among the clasts, clasts that showed the least degree of alteration were chosen for chemical analysis. In order to obtain additional geochemical data that would not be as affected by alteration, measurements of high field strength trace element abundances were also completed.

Chemical variety is seen among the BFL clasts, with SiO_2 ranging from 48% to 63%. When classified using SiO_2% and total alkalis (Le Bas et al., 1986) the clasts are basalt, basaltic andesite, or andesite (Figure 19). Similarity in enrichment of alkalis is seen in the BFL clasts compared to calc-alkaline and tholeiitic Aleutian arc volcanic rocks and the BFL clasts are more enriched in alkalis compared to MORB. The monzodiorites of Odell and Saddlebag Lakes appear more fractionated compared to the BFL clasts. When plotted on a Miyashiro (1974) type diagram, the clasts are predominantly tholeiitic similar to tholeiitic Aleutian arc volcanic rocks while the monzodiorites of Odell and Saddlebag Lakes are calc-alkaline (Figure 20). K_2O concentrations classify the BFL as medium to high K (Figure 21). Alteration experienced by the BFL clasts as measured by carbon and hydrogen analyses showed varied results. CO_2 in the BFL clasts ranges from 0.10% to 2.27% and H_2O% varies from 1.49% to 3.37% suggesting that the degree of alteration experienced by the BFL was not uniform throughout the sampled area (Table 2). Samples with prominent calcite substitution as seen in thin section correspond with increased CO2% measurement.

Trace element abundances of the BFL and the monzodiorites show enrichment in LILEs and depletion in HFSEs compared to MORB (Figure 22). LREEs such as La and Ce are enriched while HREEs Yb and Lu are depleted. Depletion of Nb and Ta relative to LILEs is seen in both the BFL clasts and monzodiorites. A positive Eu anomaly is seen in one sample of the monzodiorite which is also the most depleted in trace element concentrations in relation to the other samples making it a unique specimen.

Zircon Trace Element Geochemistry

Ten spot analyses on zircons from the monzodiorite of Odell Lake and twelve spot analyses on zircons from the monzodiorite of Saddlebag Lake were completed for this study (Table 3). Spots within the zircons were selected based on location and homogeneity of the chemical zoning. Chemical zoning within the zircon crystals is shown through CL images and the spots analyzed within the zircons ranged in CL-brightness. Areas of even CL-brightness are preferred and selected when possible to minimize the chance of analyzing spots with heterogeneous chemical compositions. U, Y, Th, and REE concentrations are higher in CL-dark zones while lower U, Y, Th, and REE concentrations characterize the CL-bright zones. Following the pattern produced by the zoning and U concentration, the zircons undulate from a U-rich core to U-poor oscillatory overgrowths with a U-rich outer rim.

The oscillatory zoning and U variation found within the zircon spot analyses shows a long thermal history and chemical fractionation in the magma body from which the zircons crystallized. Both of the monzodiorites contain zircons with a wide range of U concentrations, with the monzodiorite of Odell Lake reporting almost 1.5 times the U concentration found in the monzodiorite of Saddlebag Lake (Figure 23). When plotted against Yb, a strong positive correlation with U develops. This positive correlation exists for all of the REE when plotted against U. Using the ratio of U/Yb, less chemical variation of the zircons is seen between the zircons and between the two samples of monzodiorite (Figure 24), consistent with the collinear trend of U and Yb variation observed in these samples.

Discussion

The Triassic rock units preserved in the Saddlebag Lake pendant document the change from continental sedimentation to a landscape dominated by volcanism in the early Mesozoic. Evidence of the Antler and Sonoma orogenies are found in the basal units of the Saddlebag Lake pendant; the Triassic Candelaria formation is considered to be clastic foreland basin deposits of the Havallah basin created during the Sonoma orogeny (Schweickert and Lahren, 1987). In some locations of the Saddlebag Lake pendant, the Candelaria formation is underlain by the Permian Diablo and the Ordovician Palmetto formations, representatives from the Sonoma and Antler orogenies respectively. The tuff of Black Mountain marks the change from continent-derived sedimentation to arc volcanism and the presence of volcanism is evident even within the conglomerate of Cooney Lake with its volcanic ash-rich matrix. The tuffs of Saddlebag and Greenstone Lakes along with the BFL mark the earliest preserved record of Mesozoic volcanism following the Sonoma orogeny, indicating a change in tectonic setting along a truncated continental margin by the establishment of the east Sierran magmatic arc.

The environment of deposition of the BFL was most likely subaqueous as indicated by the clast type and interaction between the clasts and the matrix. Non-juvenile angular and sub-rounded clasts predominate in the BFL, however less common hyaloclastites and clasts with fluidal and cuspate edges indicate an interaction with fresh magma in water. Grading and undulatory structures found within the transitional units of the Saddlebag Lake Tuff suggest deposition in and interaction with water. Schweickert and Lahren (2006) also suggested a subaqueous environment of deposition based on the presence of pillowed andesites and turbidites in the Triassic section of the Saddlebag Lake pendant.

Mesozoic volcanic and volcaniclastic assemblages of the Saddlebag Lake pendant may represent the earliest record of subduction initiation and the magmatic arc built on the truncated continental margin. Determining the time of subduction initiation depends on the mechanics behind the formation of a subduction zone, which are not

completely understood as once a subduction zone becomes self-sustaining, it is not possible to infer the mode of the initiation (Stern, 2004). Two models of subduction initiation have been presented by Stern (2004; Figure 25). Induced nucleation is the continuing convergence between two plates following the failure of subduction due to a collision and the attempted subduction of buoyant crust. The evidence of this compressional event is preserved in the suturing of the buoyant crust to the original hanging wall of the subduction zone. This model also accounts for the formation of a subduction zone along a transform fault with the change in the pole of rotation leading to convergence between two plates. Spontaneous nucleation results when old dense crust spontaneously sinks and pulls the plate towards the subduction zone. Having an extensional component, spontaneous nucleation produces magmatism similar to slow spreading ridges, however magmatism produced by spontaneous nucleation is characterized by depleted tholeiites and ultra-depleted boninites (Figure 26; Stern and Bloomer, 1992). Boninites are a rare Mg-rich andesite named after Chichi-jima in the Bonin Islands and form by hydrous melting of ultra-depleted mantle (Shiraki et al., 1978; Stern, 2004). Magmatism associated with the generation of boninites in the Izu-Bonin-Mariana arc during subduction initiation was characterized by intense and widespread hydrous melting of the mantle. The presence of boninites is now used as evidence for arc initiation by spontaneous nucleation.

Spontaneous nucleation is a proposed model for the initiation of the Sierran arc during the Jurassic (Stern and Bloomer, 1992). Using the Izu-Bonin-Mariana arc as a modern analogue, Stern and Bloomer used Jurassic ophiolites as an indicator for rapidly-formed, enriched supra-subduction zone oceanic crust and an extensional environment created by spontaneous subduction initiation. However, this model of Jurassic subduction initiation is inconsistent with some evidence of Mesozoic subduction prior to the emplacement of Jurassic ophiolites. Late Triassic blueschist in the Klamath Mountains and northwestern Sierra Nevada might indicate earlier subduction initiation (Dickinson, 2000). Blueschist can be used to record subduction initiation as blueschist metamorphism occurs along the arcward flanks of accretionary prisms.

Triassic to Jurassic plutons might indicate earlier subduction initiation, though Stern and Bloomer (1992) suggested that their chemical compositions are not those expected for an immature arc.

Contrary evidence of subduction initiation is presented by Saleeby (2011) in the Kings-Kaweah ophiolite belt in the southwestern Sierra Nevada foothills. Saleeby claims that subduction initiated at a transform juncture at approximately 255 Ma based on the Sm/Nd age for metamorphism in the Kings-Kaweah ophiolite belt. Following Stern's model of spontaneous nucleation and the immediate production of boninites, Saleeby cites submarine boninitic to arc tholeiitic volcanism erupted within and above the hemipelagic cover strata covering the ophiolites at 225 to 190 Ma in support of Stern and Bloomer's model, however earlier than proposed by them. Saleeby proposes a hybridized version of Stern's induced and spontaneous nucleation models for subduction initiation suggesting that subduction began along the truncated continental margin along a transform fault. As subduction continued, slab rollback of the plate as it was entering the trench resulted in extension and the production of boninites and arc tholeiites.

Trace element geochemical signatures can be used to identify subduction initiation and the tectonic settings of andesitic rocks produced in island arcs above a subduction zone (Bailey, 1981). Possible tectonic settings for the generation of andesites include oceanic island arcs and continental island arcs on either thin or thick crust. Arc lavas are enriched in large ion lithophile elements (LILE) which are fluid-mobile and incompatible in the subducting crust. Enrichment of light rare earth elements (LREE), U, Th, and Pb is also seen in magmatic arcs, as these elements behave similarly to LILE. High field strength elements (HFSE) such as Nb, Ta, Zr, Hf and the heavy rare earth elements (HREE) are less fluid-mobile and less enriched in arc lavas. Greater enrichment of LILE, LREE, U, Th, and Pb are seen in arcs generated above continental crust, with thicker crusts resulting in the greatest enrichment (Hildreth and Moorbath, 1988). Enrichment in fluid-mobile elements can be used to show the evolution of a magmatic arc. As the subducted plate continues to subduct, dehydrating

and carrying fluid-mobile LILE into the mantle, a magmatic arc becomes established. As the magmatic arc matures, increased enrichment in fluid mobile elements is seen over time (Hildreth and Moorbath, 1988, Ishizuka et al., 2006).

Stern's model of spontaneous nucleation for the initiation of the Sierra Nevada magmatic arc would necessitate the same mechanism and resulting rock record as produced by the cited modern analogue, the Izu-Bonin-Marianas arc. Spontaneous nucleation first produces boninites, Mg rich, silica saturated andesites. Following the initial boninitic volcanism, the arc matures to produce andesites that are increasingly enriched in LILE as the arc matures. To determine the maturation of the magmatic arc that produced the BFL clasts, possibly a nascent arc, boninites and andesites representing the development and evolution of the Izu-Bonin-Mariana are compared to the BFL clasts: boninites dated at 47.9 ± 0.4 Ma, andesites ranging in age from 42 to 44 Ma, and andesite representing the most mature magmatic arc erupted between 1883 to 1981 (Taylor et al., 1993; Ishizuka et al., 2006; Elliott et al., 1997). The 47.9 ± 0.4 Ma boninite represents the earliest record of arc initiation (Reagan et al., 2008). The andesite that is dated to 42-44 Ma represents the change from boninitic to andesitic lavas and the maturation of the subduction zone. Finally the fresh andesite erupted from 1883 to 1981 represents the most chemically evolved arc lava. By using the samples that represented the evolution of the subduction zone in both age and composition, the evolutionary stage of the magmatic arc that produced the BFL clasts can be determined.

Arc generated lavas are enriched in LILE and LREE and are depleted in HFSE (Elliott et al., 1997). The boninites and andesites produced by a magmatic arc show these enrichments and depletions (Figure 27). Increased enrichment in andesites produced by the Izu-Bonin-Mariana arc is shown as the arc matures. The BFL clasts show enrichments and depletions similar to those observed in Izu-Bonin-Mariana lavas, implying a magmatic arc affinity; however, the BFL clasts more closely match the enrichments seen in the mature modern andesite.

Continental magmatic arcs generated above continental crust result in greater enrichment in trace element concentrations (Bailey, 1981) and could provide a better match for the BFL clasts. The thickness of the crust on which the island arc was produced can be determined by the enrichment of trace element concentrations. This is well illustrated by the magmatic arc that composes the Southern Volcanic Zone of the Andes as the thickness of the crust increases northward along the magmatic arc (Hildreth and Moorbath, 1988). The trend of increasing continental thickness and correlated trace element enrichment is seen beyond the Southern Volcanic zone and continues through the entire stretch of the Andes. Comparing andesites from volcanos representing the thick crust (≥ 50 km) Northern and Central Volcanic Zones and the thin crust (~30 km) Southern Volcanic Zone of the Andes can illustrate the influence of crustal thickness on the enrichment of trace elements (Figure 28; Feininger and Seguin, 1983; Hickey-Vargas et al.,1989; Hildreth and Moorbath, 1988; Hora et al., 2007; Mamani et al., 2009; Monzier et al., 1999). The Southern Volcanic Zone is represented by Quetrupillan volcano, an inactive stratovolcano built on crust approximately 30 km thick (Hickey-Vargas et al., 1989; Hildreth and Moorbath, 1988). Parinacota volcano is a stratovolcano built on 70 km thick crust in the Central Volcanic Zone and was active until 20 ka (Hora et al., 2007; Mamani et al., 2009). The Northern Volcanic Zone is represented by the still active Sangay volcano built on crust greater than 50 km thick (Monzier et al., 1999). Sangay, located in Ecuador, is the most active volcano in the Northern Volcanic Zone in the Andes and one of the most active andesitic volcanoes in the world (Monzier et al., 1999). The complex is composed of three edifices, the older two have been destroyed by sector collapses. The third and youngest edifice has a minimum age of 14 Ka and is 9 by 10 km in size with an almost a perfect cone with sides that slope at 35°. Lava and pyroclastic flows have been documented since 1628 and only minor activity has been recorded since the last large eruption in 1942. Sangay is unique among the volcanos in the Northern Volcanic Zone as it has the highest K_2O, Na_2O, Rb, Ba, La, Th, Sr, and Nb concentrations, correlating with the increase of incompatible elements inward and away from the trench.

Magmatic arcs built on thick continental crust exhibit greater concentrations of Rb, Cs, Ba, Th, and LREE then arcs built on thin continental crust (Hildreth and Moorbath, 1988). The thick crusted Northern and Central Volcanic Zone andesites show the largest enrichment and the best match for the BFL. Despite the incomplete trace element data available for Sangay, the similarities in enrichments and depletions between Sangay and the BFL clasts is striking (Figure 29).

When combined with the whole rock geochemistry of the clasts from the BFL, zircon geochemistry of zircons from the monzodiorites of Odell and Saddlebag Lakes complete the picture of the change from continental sedimentation to volcanism and magmatism during the early Triassic. Geochemical signatures used to determine magmatic arc petrogenesis in whole rock data are applicable to zircon geochemistry as well, since HFSE and rare earth elements (REE) are available to substitute into the structure of zircons during crystallization. The structure of zircon allows for the substitution of REE along with Y, Th, U, Hf, Nb and Ta providing a geochemical and geochronological record that is practically impervious to the geologic cycle (Belousova et al., 2006; Grimes et al., 2007). With the availability of HREE, Y, Hf, Th, and U to be substituted in zircon, the geochemical behavior of the enrichment and depletion of these elements in arc lavas compared to depleted mid-ocean ridge basalt (MORB) in whole rock geochemistry can be applied to zircon geochemistry as well. In arc lavas, LREE, U, Th, and Pb are enriched while the middle to heavy REE are depleted relative to MORB (Elliott et al., 1997; Kelemen et al., 2003). The LREE along with U, Th, and Pb behave similar to the large ion lithophile elements (LILE) which are fluid-mobile and incompatible in the subducting crust, producing magmatic arcs constructed of volcanic rocks that have high LILE abundances (Elliott et al., 1997). Enrichment in LREE, U, Th, and Pb in zircon geochemistry parallels the enrichment in LILE seen in whole rock geochemistry for magmatic arcs (Grimes et al., 2007). It is possible to recognize this enrichment in zircons produced by magmatic arcs and distinguish zircons produced by a magmatic arc from zircons formed at a mid-ocean ridge.

In addition to whole rock trace element geochemistry, magmatic arc signatures can be recorded and discerned in the geochemistry of zircon as well. Zircons collected from two monzodiorites from the Saddlebag Lake pendant suspected to have been produced in a magmatic arc were compared to zircons from modern mid-ocean ridge gabbros (MORG) in an attempt to discriminate between zircons crystallized in a magmatic arc setting and MORG zircons. Zircons collected from the monzodiorites show substantial compositional overlap in actinide and REE data. MORG data from Grimes et al. (2007) represents zircon analyses from gabbro formed in young ocean crust along the Mid-Atlantic Ridge. As demonstrated by Grimes et al. (2007), REE element abundances of zircons from most rock types overlap (Figure 30) and cannot be used to distinguish tectonic setting. To complete a more conclusive analysis in the attempt to discriminate between magmatic arc and mid-ocean ridge affinity, fluid mobile elements, such as U, are more informative. Enrichment in U suggests that the zircon was crystallized from magma generated at a magmatic arc as LILE are more enriched in rocks formed in a magmatic arc (Elliot et al., 1997).

MORG U concentrations vary between the three rock types reflecting the compositional differences of the rocks, however U concentrations are depleted when compared to the monzodiorites. When fluid mobile and immobile element abundances are compared between zircons from the monzodiorites and MORG, the consistently high U and low Yb concentrations in the monzodiorites are apparent (Figure 31). Ratios of fluid mobile over fluid immobile elements produce similar results (Figure 32). Based on the concentration of U, the monzodiorites are chemically distinct from MORG and enrichment of U in the monzodiorites indicates a magmatic arc petrogenesis.

When compared to other zircons generated by a magmatic arc, the monzodiorites show similar U and Yb concentrations, suggesting a magmatic arc petrogenesis for the monzodiorites. For example, the Talkeetna Formation and associated plutonic rocks in the Chugach Mountains of south-central Alaska are interpreted based on whole rock compositions to be the remnants of a relatively primitive, low-Al oceanic magmatic arc, the Talkeetna arc (DeBari and Sleep, 1991;

Kelemen et al., 2003). This remnant arc formed by subduction along the margin of North America in Jurassic time. Grimes et al. (2007) showed that zircons recovered from tonalite to quartz diorite dikes in the Talkeetna arc have high U and low Yb contents compared to MORG zircons. Both the monzodiorites analyzed in this study and the Talkeetna arc zircons are equally enriched in U and have high U/Yb when compared to MORG zircons (Figure 33).

Conclusions

The environment of deposition of the BFL is recorded by the transitional units deposited immediately prior to breccia deposition, and by the clasts of the BFL. Preserved, unaltered quartz and the absence of glass shards or bubble walls in the transitional units indicate that the tuff has gone through diagenesis. This is supported by the undulatory layers seen in the transitional units as a welded tuff would not allow a free surface to be reworked by water. The BFL is composed of angular and non-juvenile clasts, including some hyaloclastites. Fluidal and cuspate borders of the clasts from the BFL suggest a subaqueous, not necessarily marine, depositional environment with the mixing of preexisting and fresh hot magma.

Constrained in age between the 223 Ma tuff of Saddlebag Lake and the 220 Ma tuff of Greenstone Lake, the BFL represent tholeiitic volcanism from a non-nascent magmatic arc that was well established in the early Triassic. The BFL are undoubtedly from a magmatic arc however the trace element concentrations of the BFL are more enriched than the depleted andesites and very depleted boninites from the Izu-Bonin-Mariana arc. The BFL failed to match boninites in trace element enrichment and are unlikely the products of a nascent subduction zone. Based on the similarities in enrichment between the BFL and Sangay volcano in Ecuador, the BFL were most likely produced by a continental island arc built on thick crust approximately 50 km thick. Considering the age constraints on the emplacement of the BFL by the tuff layers found on either side along with the geochemical data presented here, the magmatic arc that created the BFL was already established in the Triassic and built on thick crust. This evidence continues to contradict the Jurassic ophiolites in northern California used to correlate subduction initiation by spontaneous nucleation between 164 to 153 Ma by Stern (2004). Despite citing evidence of subduction establishment prior to 164 Ma, Stern believes that sufficient proof exists to place subduction initiation by spontaneous nucleation in the late Jurassic.

Contrary evidence of subduction initiation is presented by Saleeby (2011) in the Kings-Kaweah ophiolite belt in the southwestern Sierra Nevada foothills. Saleeby claims

that subduction initiated at a transform juncture at approximately 255 Ma based on Sm/Nd age for metamorphism in the Kings-Kaweah ophiolite belt and arc magmatism related to the nascent subduction zone began at 248 Ma in the eastern Sierra. Following Stern's model of spontaneous nucleation and the immediate production of boninites, Saleeby cites submarine boninitic to arc tholeiitic volcanism erupted within and above the hemipelagic cover strata covering the ophiolites at 225 to 190 Ma in support of Stern's model, however earlier than proposed by Stern. Not completely discounting Stern's proposed model of subduction initiation by spontaneous nucleation, Saleeby suggests that the actual model was a hybridization of Stern's spontaneous nucleation and induced spontaneous initiation models (Figure 25).

In addition to providing information regarding tectonic setting, zoned zircons are capable of recording variations in the chemical composition of the melt from which they crystallized. The range of U concentrations in zircons from the monzodiorite of Odell Lake and the monzodiorite Saddlebag Lake indicates changing chemical compositions during crystallization in an evolving magma system. Oscillatory chemical zoning of the zircons in this study indicates changing levels of actinide and REE enrichment reflecting the changing melt chemistry in the magma conduit. The preservation of melt-chemistry provides a link to magmas that has erupted from the system. Mafic volcanic rock clasts from the BFL correlate temporally with the monzodiorites of Odell and Saddlebag Lakes and could represent such erupted products. The chemistry of the melt preserved in the monzodiorite zircons can be used to link the volcanic clasts from the BFL to the magma chamber, now exposed as the monzodiorites of Odell and Saddlebag Lakes.

Table 1. U/Pb geochronology of intrusive and extrusive rocks completed for this study.

Rock Unit	**206Pb*/238U age (Ma)**
monzodiorite of Saddlebag and Odell Lakes	220+/-2 Ma
tuff of Greenstone Lake	220+/-2 Ma
tuff of Saddlebag Lake	223+/-2 Ma

Table 2. Measured major and trace element abundances in breccia of Frog Lakes clasts.

Sample (XRF)	C	CC	CD	CF	CK	CL	CN	CQ	CZ
SiO2 (%)	51.5	49.56	53.58	57.92	55.23	56.97	48.71	54.57	63.39
TiO2 (%)	0.78	0.84	0.66	0.71	0.69	0.73	0.99	0.77	0.67
Al2O3 (%)	18.19	20.07	16.37	16.57	16.89	17.3	20.75	18.07	16.22
Fe2O3 (%)	9.1	8.55	8.42	7.7	7.84	8.55	10.32	8.44	5.48
MnO (%)	0.25	0.23	0.25	0.16	0.18	0.14	0.28	0.19	0.1
MgO (%)	4.37	3.74	3.39	3.02	2.34	1.87	4.23	3.06	1.64
CaO (%)	6	7.11	7.48	5.34	6.99	5.08	4.1	7.38	4.48
Na2O (%)	4.48	4.18	3.28	3.41	4.41	2.36	5.57	2.67	3.44
K2O (%)	0.68	1.5	1.41	2.08	1.42	3.2	0.97	1.13	2.02
P2O5 (%)	0.35	0.37	0.31	0.32	0.32	0.33	0.45	0.35	0.31
Totals	95.7	96.15	95.15	97.23	96.31	96.53	96.37	96.63	97.75
LOI (%)	4.12	3.58	4.6	2.57	3.45	3.22	3.42	3.17	2.01
CO2%	1.25	0.11	1.94	0.16	1.28	0.71	0.10	0.57	2.27
H2O%	2.54	2.70	2.29	1.50	1.49	1.72	3.37	2.31	1.19
Ni (PPM)	0	0	0	0	0	0	0	2	0
Cu (PPM)	23	31	22	35	9	17	9	67	10
Zn (PPM)	93	92	92	63	54	59	134	77	41
Rb (PPM)	27	59	63	89	56	132	32	49	81
Sr (PPM)	973	1143	1033	670	1041	567	787	765	749
Zr (PPM)	82	92	73	83	76	89	96	91	108
Ba (ICP)	500	1255	1218	982	1031	1629	1051	904	1307
La	27.5	34.7	25.2	28.3	26.1	35.7	28.1	27.7	29.3
Ce	56.3	68.8	49.7	55.6	52.3	68.7	60.8	56.1	59.3
Pr	6.95	8.45	6.21	6.85	6.54	8.37	7.88	7.04	7.2
Nd	28.1	32.9	25.1	27.2	26.4	32.1	32.8	28.3	29.1
Sm	5.94	6.96	5.32	5.69	5.53	6.43	7.29	6.04	6.16
Eu	1.55	2.06	1.46	1.55	1.5	1.97	1.63	1.53	1.51
Gd	5.34	6.05	4.67	5.01	4.88	5.6	6.67	5.25	5.64
Y	25.02	28.27	21.24	23.93	23.16	24.26	30.66	25.41	28.88
Dy	4.19	4.74	3.86	4.05	3.99	4.31	5.45	4.26	4.57
Ho	0.89	0.96	0.77	0.82	0.81	0.86	1.09	0.89	0.93
Er	2.53	2.68	2.22	2.32	2.32	2.36	2.98	2.51	2.6
Lu	0.39	0.41	0.32	0.35	0.36	0.34	0.45	0.38	0.4
Yb	2.6	2.83	2.17	2.32	2.4	2.29	3.03	2.55	2.65
Tb	0.77	0.87	0.69	0.73	0.72	0.79	0.97	0.77	0.82
V	142.29	147.27	118.6	162.96	128.48	154.71	131.98	141.84	113.27
Cr	3.11	4.11	3.02	3.01	3.06	3.22	1.35	4.09	3.6
Nb	7.72	9.04	7.17	7.42	7.15	7.57	9.08	7.67	10.28
Hf	2.7	2.8	2.5	2.4	2.4	2.6	3.2	2.7	2.9
Ta	0.44	0.53	0.4	0.46	0.45	0.56	0.69	0.44	0.67
Pb	9.2	18.3	19.4	10.1	17.9	8.2	10.7	9.2	11.6
Th	6.1	6.8	6.0	5.8	6.1	6.3	6.6	6.4	6.9
U	1.8	2.3	1.6	1.4	1.8	1.7	1.7	1.9	2.2

Table 3. Rare earth element, Y and actinide element abundances in zircons from the monzodiorite of Odell Lake, the monzodiorite of Saddlebag Lake, and the Madagascar zircon standard.

	Y	La	Ce	Nd	Sm	Eu	Gd	Dy	Er	Yb	lHf	Th	U
Monzodiorite of Odell Lake													
736-1	923.12	0.03	9.91	1.82	3.58	0.37	26.16	93.54	163.97	287.00	8894.87	178.99	350.34
736-2	1526.12	0.07	13.35	3.10	5.93	0.64	45.55	148.20	260.78	431.73	8888.54	299.69	510.83
736-3	751.00	0.23	9.73	1.19	2.61	0.27	19.26	72.58	132.51	243.49	9163.73	141.92	358.12
736-4	767.85	0.02	10.27	1.06	2.68	0.28	19.77	74.03	137.55	258.95	8702.63	147.69	376.68
736-5	1741.95	1.19	20.17	3.50	7.15	0.74	52.48	177.34	300.30	503.35	9031.10	513.59	779.27
736-6	1427.55	0.07	13.54	2.76	5.19	0.57	42.18	142.69	239.80	396.10	9154.78	346.97	567.66
736-7	1166.88	0.05	11.59	2.38	4.80	0.51	35.85	119.51	201.13	339.23	8930.07	225.44	385.64
736-8	1593.91	0.28	17.84	2.78	6.00	0.45	44.65	156.24	276.09	463.03	9907.87	452.98	874.86
736-9	2197.32	0.10	26.67	3.89	9.40	0.84	67.38	227.87	373.97	608.94	8875.49	849.95	1087.60
736-10	770.21	0.03	8.37	1.36	3.16	0.33	22.47	76.45	136.02	243.20	8547.03	126.18	277.28
Monzodiorite of Saddlebag Lake													
AB08733-1.1	799.90	0.02	9.52	1.10	2.78	0.38	22.41	81.14	144.41	246.16	9575.55	153.45	305.53
AB08733-10.1	1142.66	0.02	10.76	2.51	5.47	0.64	36.70	123.24	202.52	330.93	9779.32	217.00	381.60
AB08733-11.1	545.92	0.02	7.95	0.46	1.43	0.19	12.16	51.28	96.33	179.41	9790.43	94.10	222.63
AB08733-12.1	442.20	0.18	8.36	0.61	1.03	0.16	9.43	40.36	80.98	158.03	9917.88	85.04	239.19
AB08733-2.1	463.94	0.03	7.66	0.35	1.09	0.17	10.48	43.15	82.98	157.22	9745.74	87.91	221.39
AB08733-3.1	539.46	0.02	10.57	0.43	1.27	0.14	12.02	50.40	98.40	181.52	10023.03	109.05	259.36
AB08733-4.1	333.80	0.02	6.46	0.29	0.82	0.12	7.69	32.71	65.26	123.45	10028.94	71.44	191.44
AB08733-5.1	979.57	0.01	11.10	1.16	3.41	0.44	29.28	101.75	179.18	305.37	9770.10	194.95	376.28
AB08733-6.1	477.98	0.02	8.69	0.34	1.01	0.14	9.91	43.62	89.81	173.01	10233.22	95.66	257.24
AB08733-7.1	509.49	0.02	9.65	0.54	1.41	0.20	13.08	50.71	92.41	168.35	9264.86	110.04	245.85
AB08733-8.1	1492.71	0.04	13.37	3.28	6.34	0.58	42.67	150.11	265.89	440.74	9970.10	350.88	640.78
AB08733-9.1	839.86	0.03	9.23	1.58	3.16	0.42	24.30	84.60	150.14	263.52	8743.73	169.35	333.59
Standard (Madagascar Green)													
MAD-5.1	1016.10	0.03	134.14	2.26	4.50	0.40	27.40	89.44	160.75	345.71	16623.19	1108.68	4432.13
MAD-10.1	910.88	0.05	141.26	2.13	4.40	0.33	25.83	81.68	145.76	305.27	15765.33	1217.20	3959.81
MAD-6.1	995.04	0.04	134.91	2.39	4.47	0.36	26.10	87.76	158.56	337.51	16215.35	1114.85	4344.47
MAD-1.2	928.69	0.03	141.55	2.05	4.20	0.36	25.03	82.74	148.02	312.94	16114.91	1191.64	4044.56
MAD-4.1	949.30	0.04	143.14	2.06	4.23	0.36	25.64	83.39	151.91	323.57	16681.22	1197.65	4219.03
MAD-1.2	928.69	0.03	141.55	2.05	4.20	0.36	25.03	82.74	148.02	312.94	16114.91	1191.64	4044.56
MAD-4.1	949.30	0.04	143.14	2.06	4.23	0.36	25.64	83.39	151.91	323.57	16681.22	1197.65	4219.03

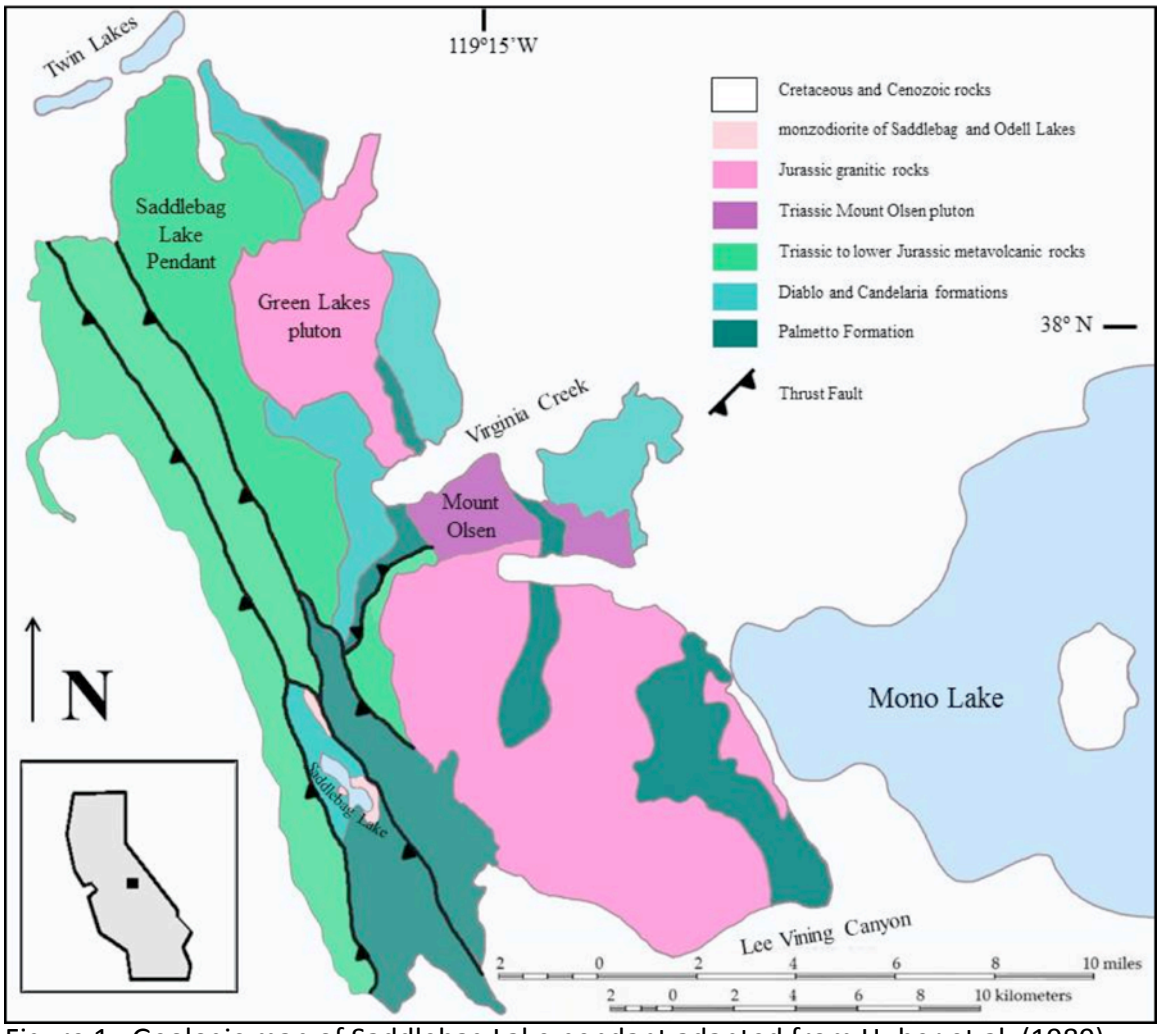

Figure 1. Geologic map of Saddlebag Lake pendant adapted from Huber et al. (1989), Koenig (1963), Schweickert and Lahren (1987, 1999), and Strand (1967).

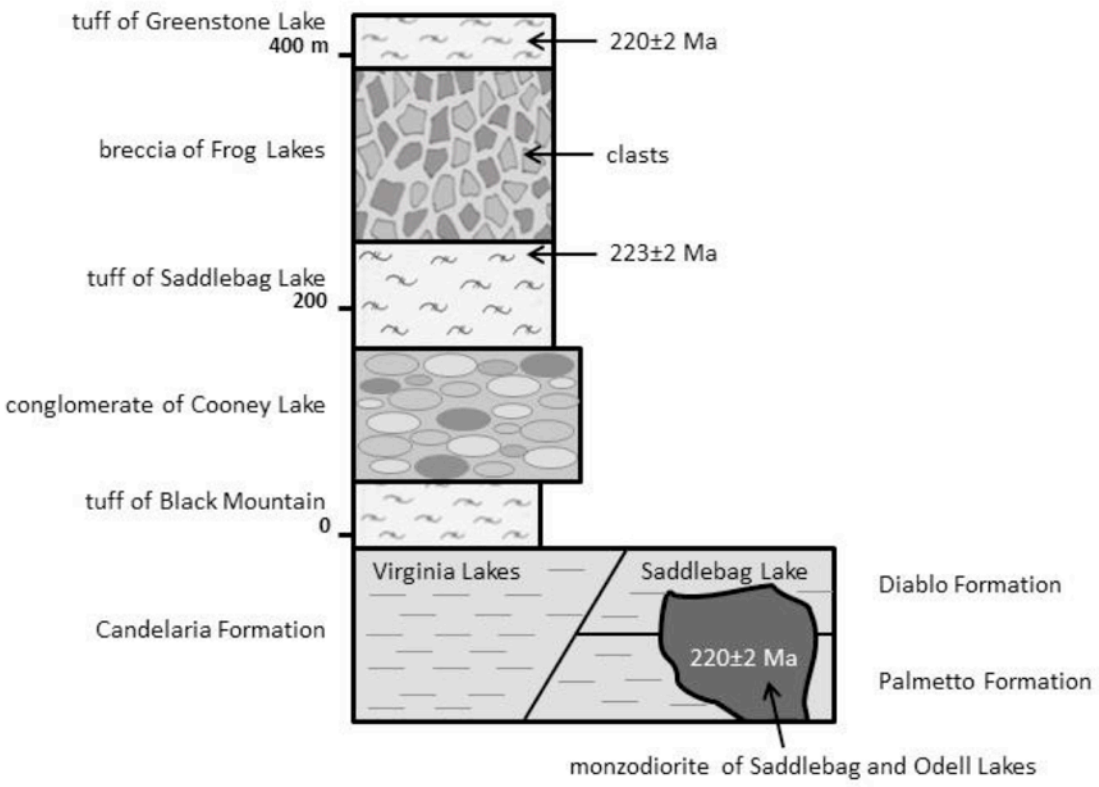

Figure 2. Stratigraphic column of the Saddlebag Lake pendant at Virginia Lakes and Saddlebag Lake (Barth et al., 2011).

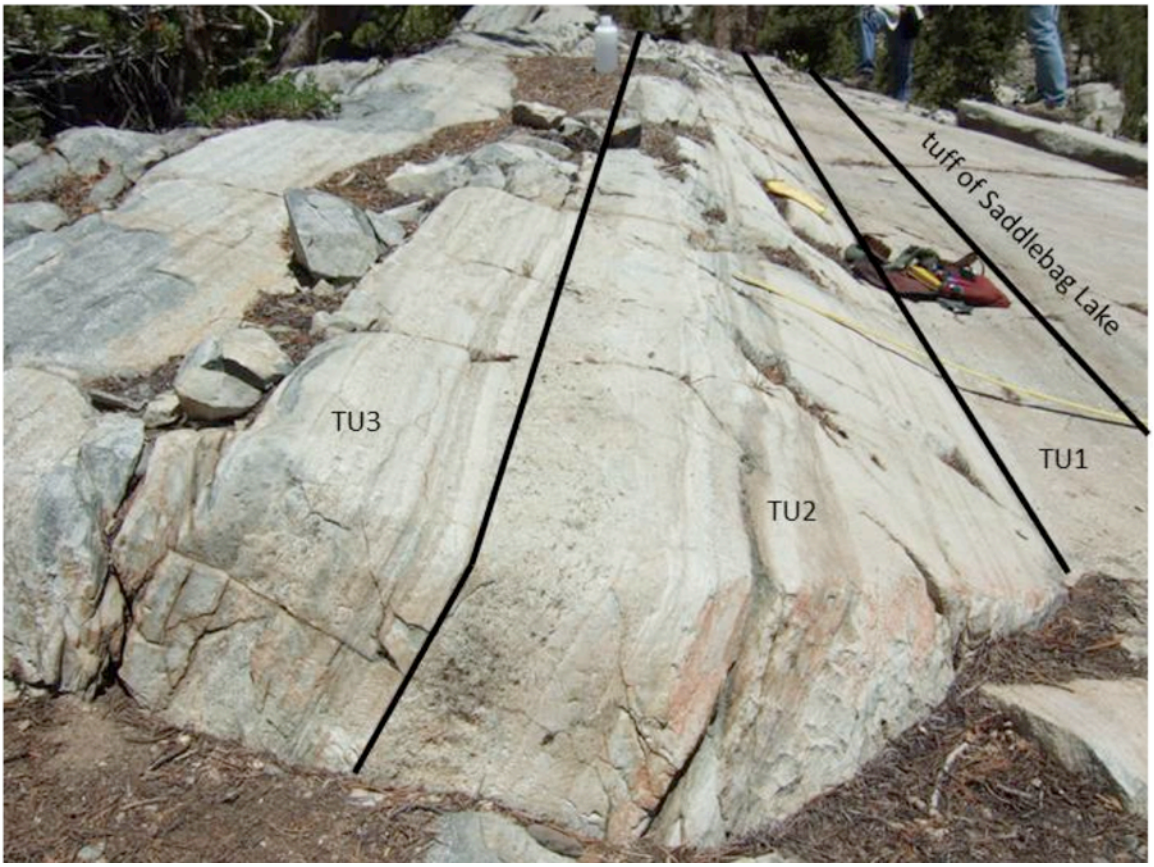

Figure 3. Transitional units 1 through 3 (view north).Tuff of Saddlebag Lake is to the right, transitional units 4 through 5 followed by the breccia of Frog Lakes and the tuff of Greenstone Lake are to the left. Meter stick and people for scale.

Figure 4. The base of the first transitional unit has reverse coarsening. Meter stick for scale.

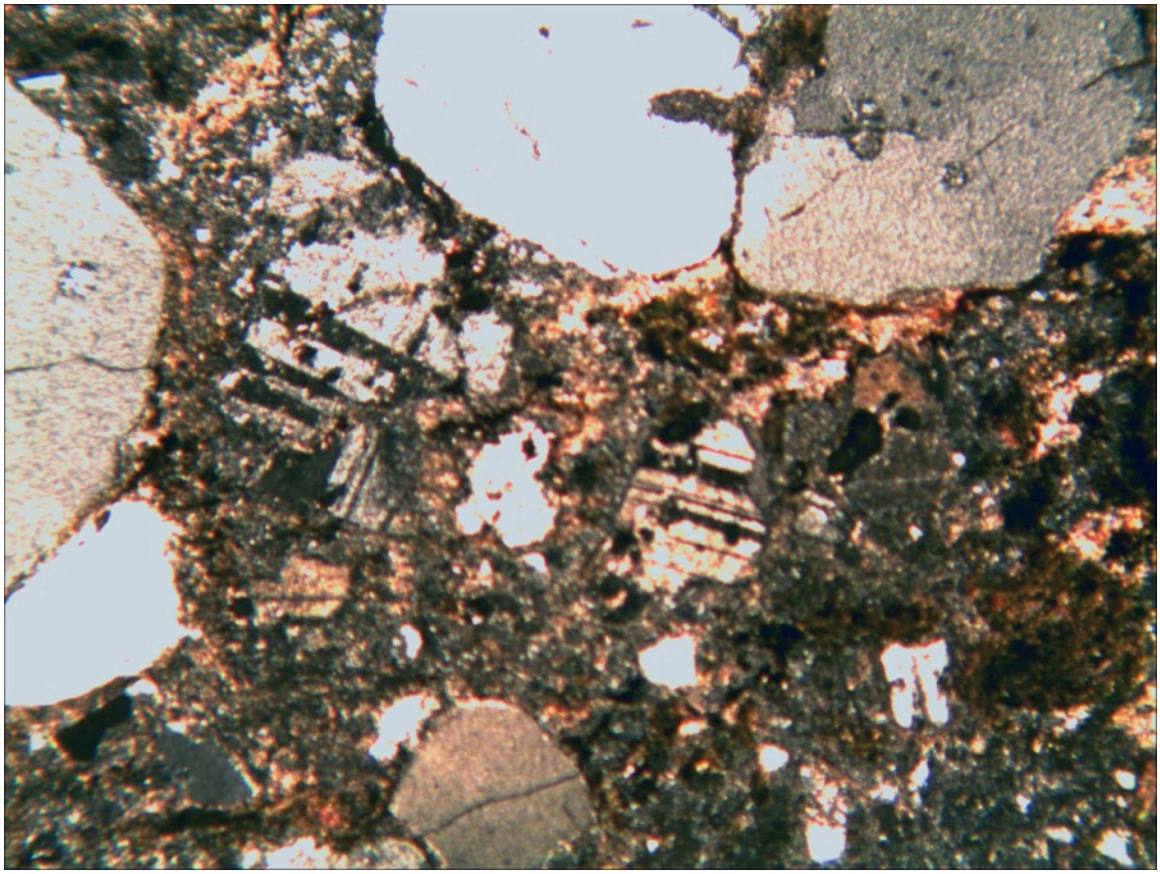

Figure 5. Embayed quartz and plagioclase phenocrysts in the first transitional unit. 40x magnification with a field of view equal to approximately 6 mm^2.

Figure 6. The base of second transitional unit channels into the underlying first transitional unit. Hammer is 31.5 cm long.

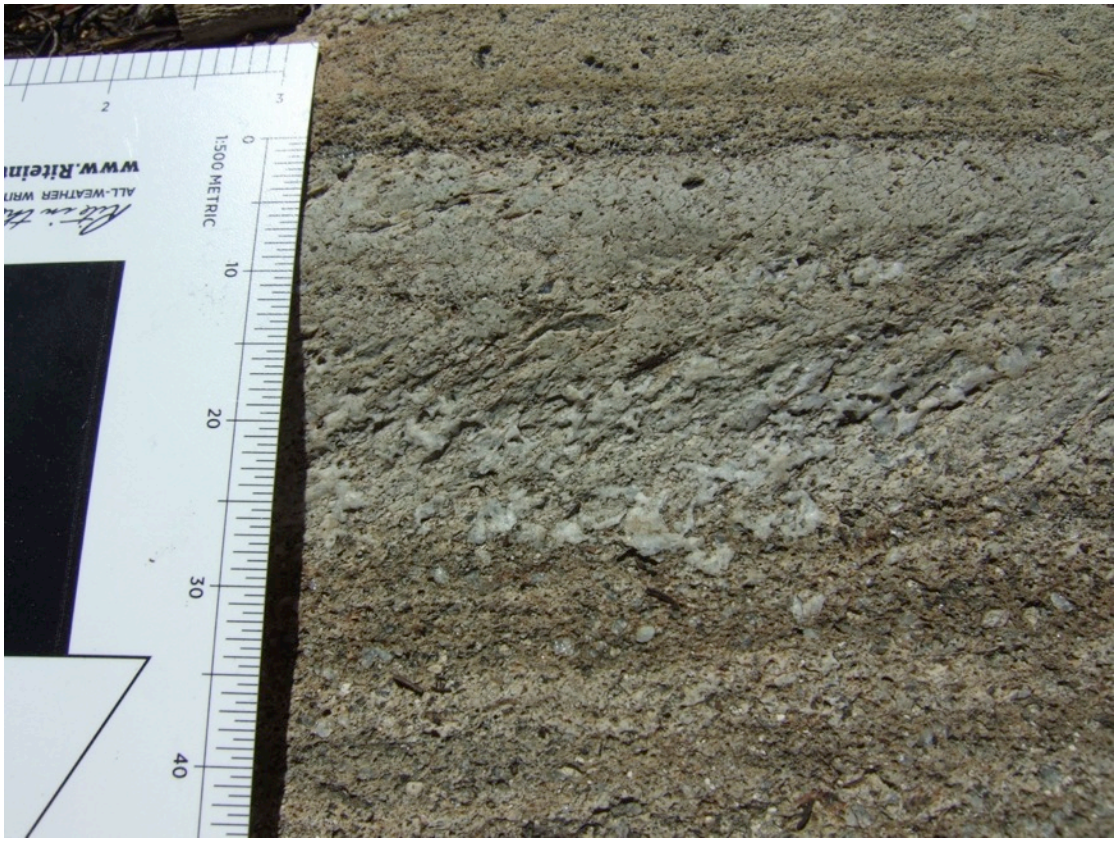

Figure 7. Feldspar and quartz phenocrysts in transitional unit 2.

Figure 8. Alternating banding with no grading is seen in the base of transitional unit 3.

Figure 9. Subhedral plagioclase phenocrysts 1-3 mm long in transitional unit 3.

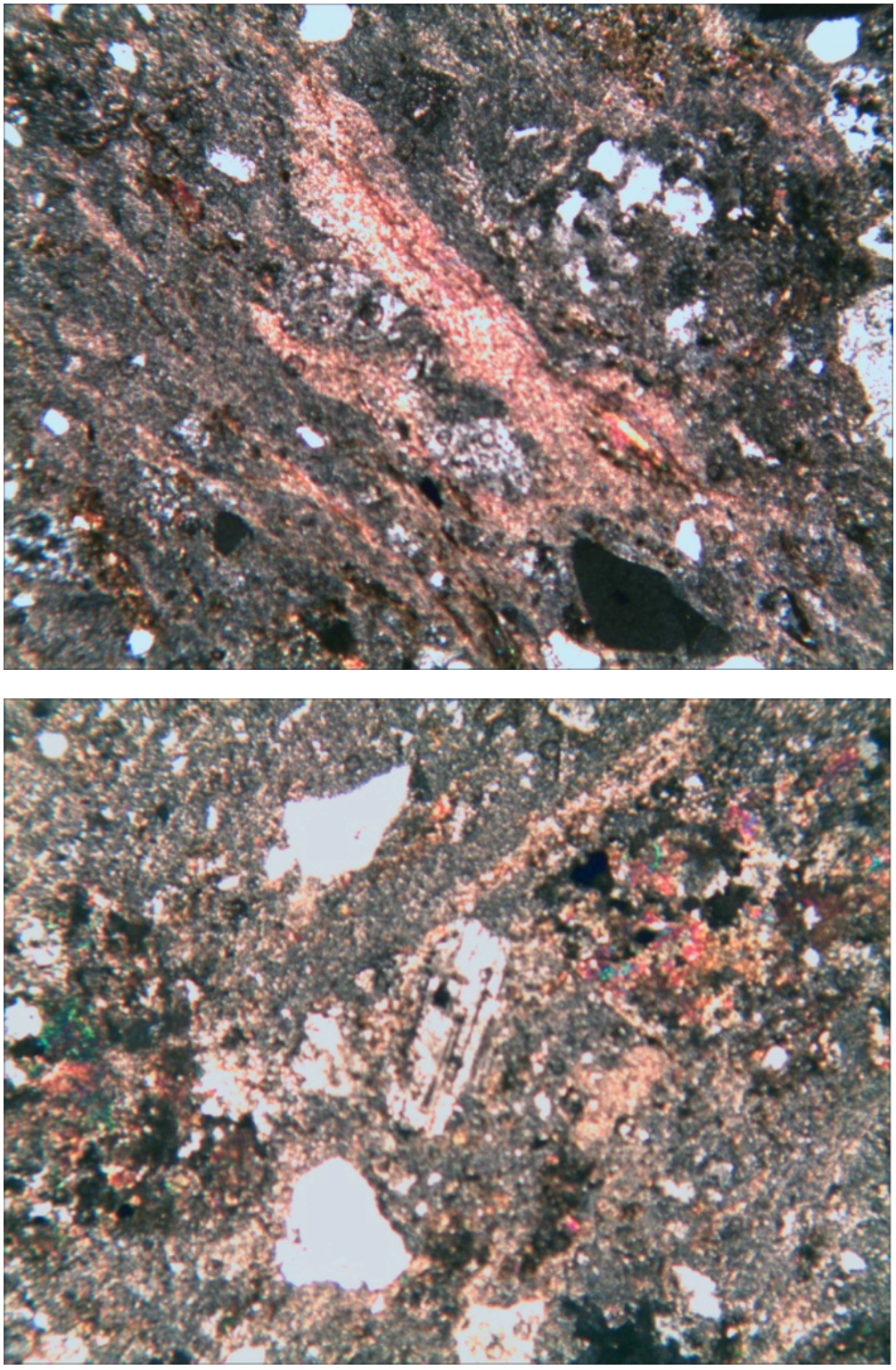

Figure 10. Transitional unit 4. 40x magnification with a field of view equal to approximately 6mm^2.

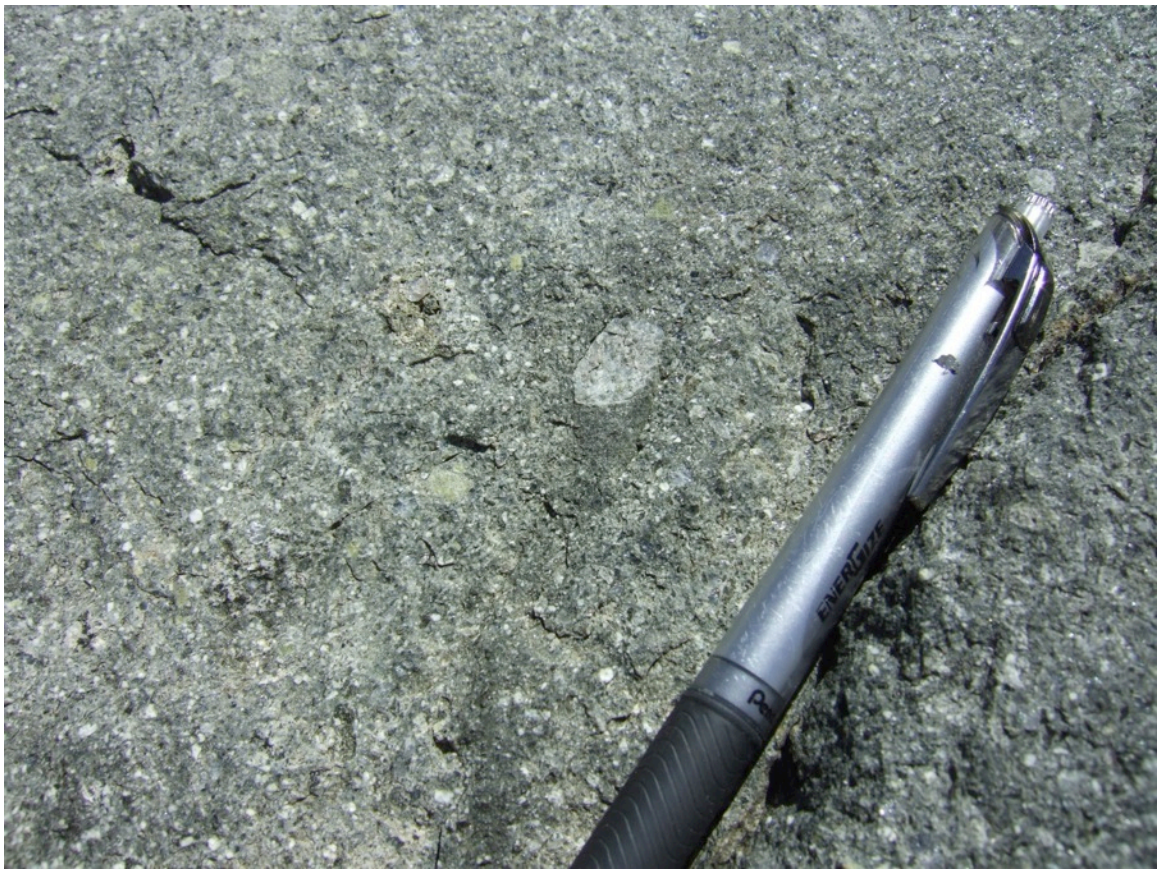

Figure 11. Structureless transitional unit 5. Silver section of pencil is 8.5 cm long.

Figure 12. Angular to subrounded clasts in the breccia of Frog Lakes. Hammer is 31.5 cm long.

Figure 13. Fluidal and cuspate borders between clasts and matrix in the breccia of Frog Lakes. Pen is 13.5 cm long.

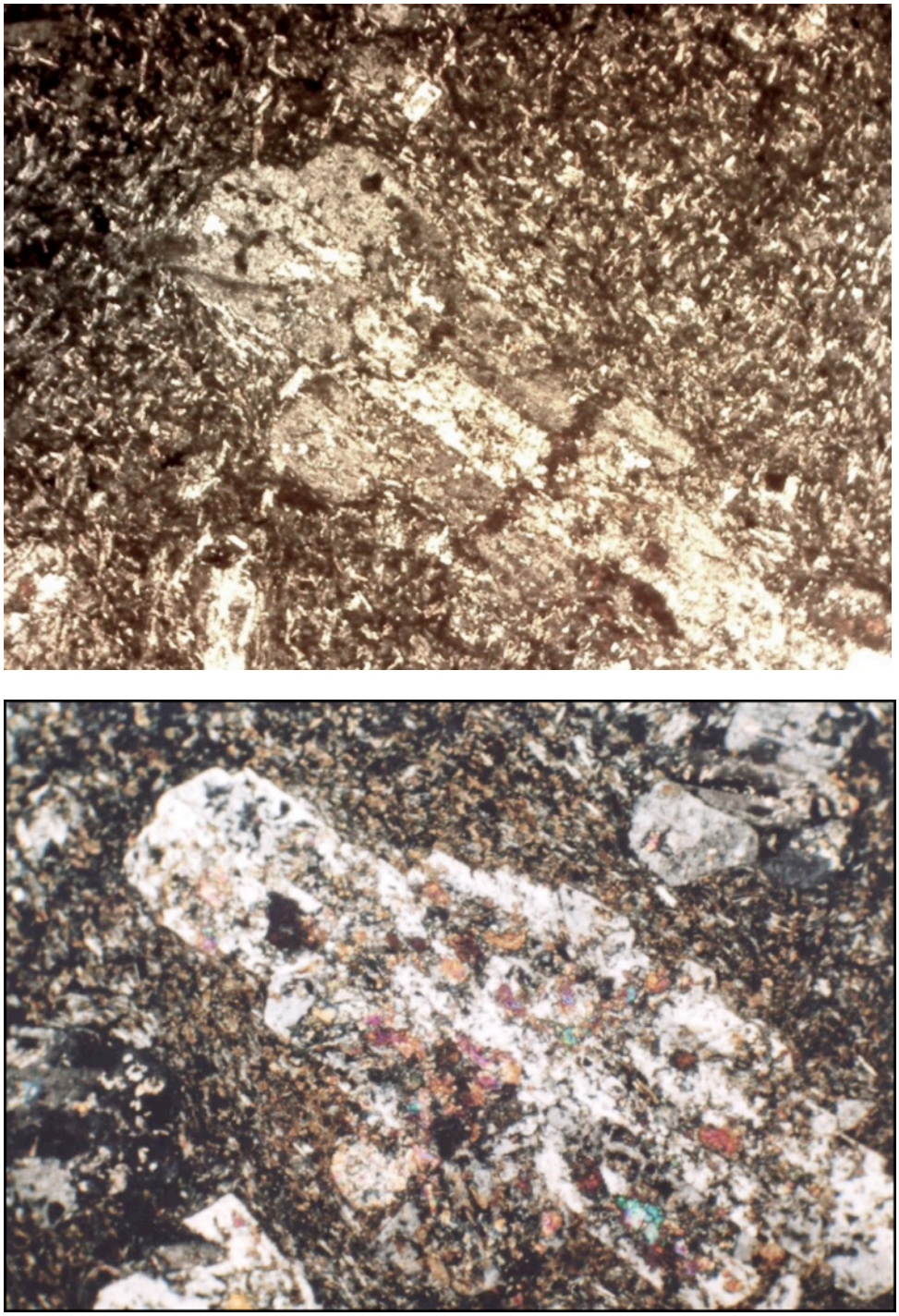

Figure 14. Preservation of original matrix texture is seen in petrographic examination of breccia of Frog Lakes clasts along with greenschist facies alteration of plagioclase phenocrysts. 40x magnification with a field of view approximately 6mm^2.

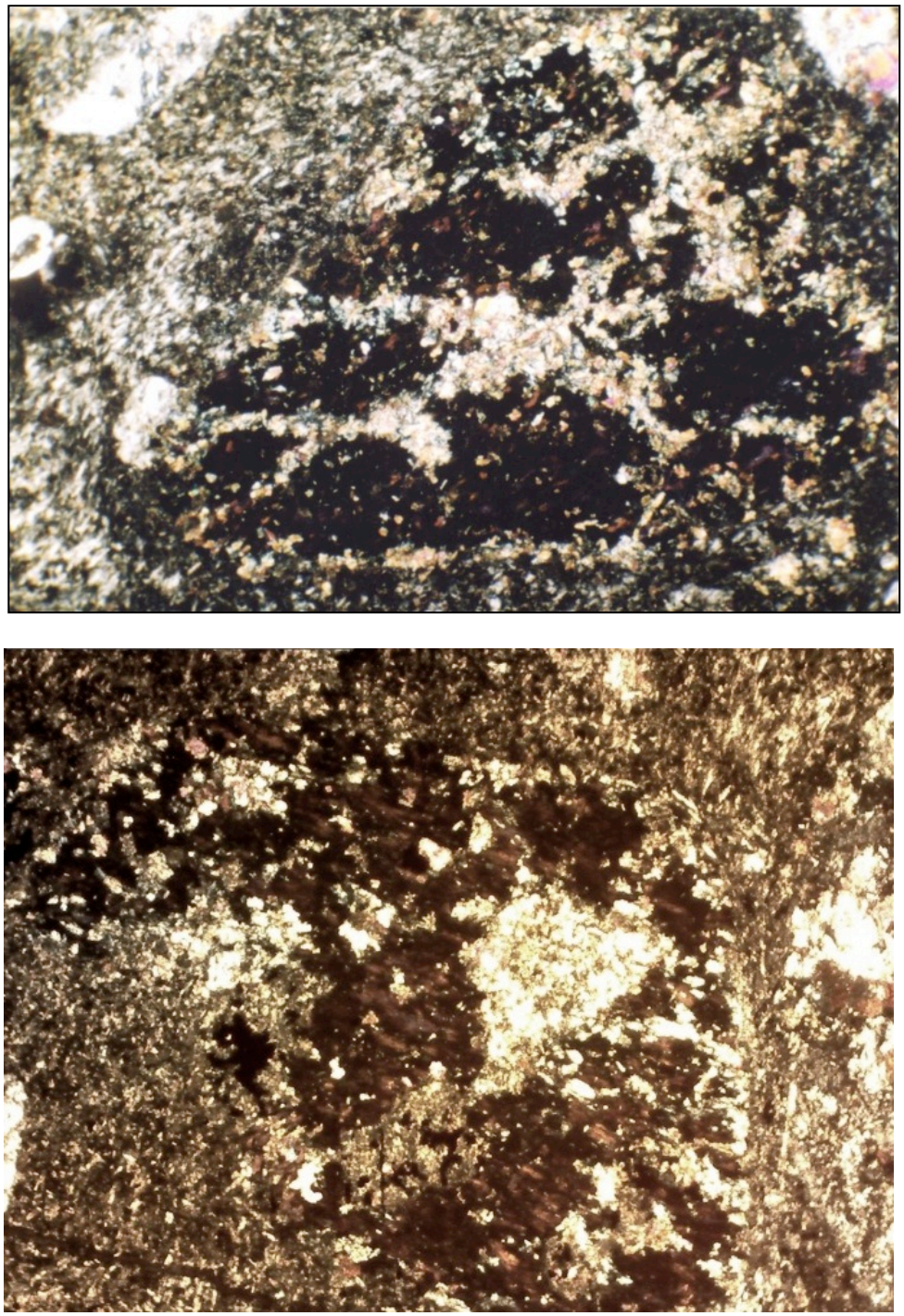

Figure 15. Alteration of hornblende phenocrysts to chlorite in the breccia of Frog Lakes clasts. 40x magnification with a field of view approximately 6mm^2.

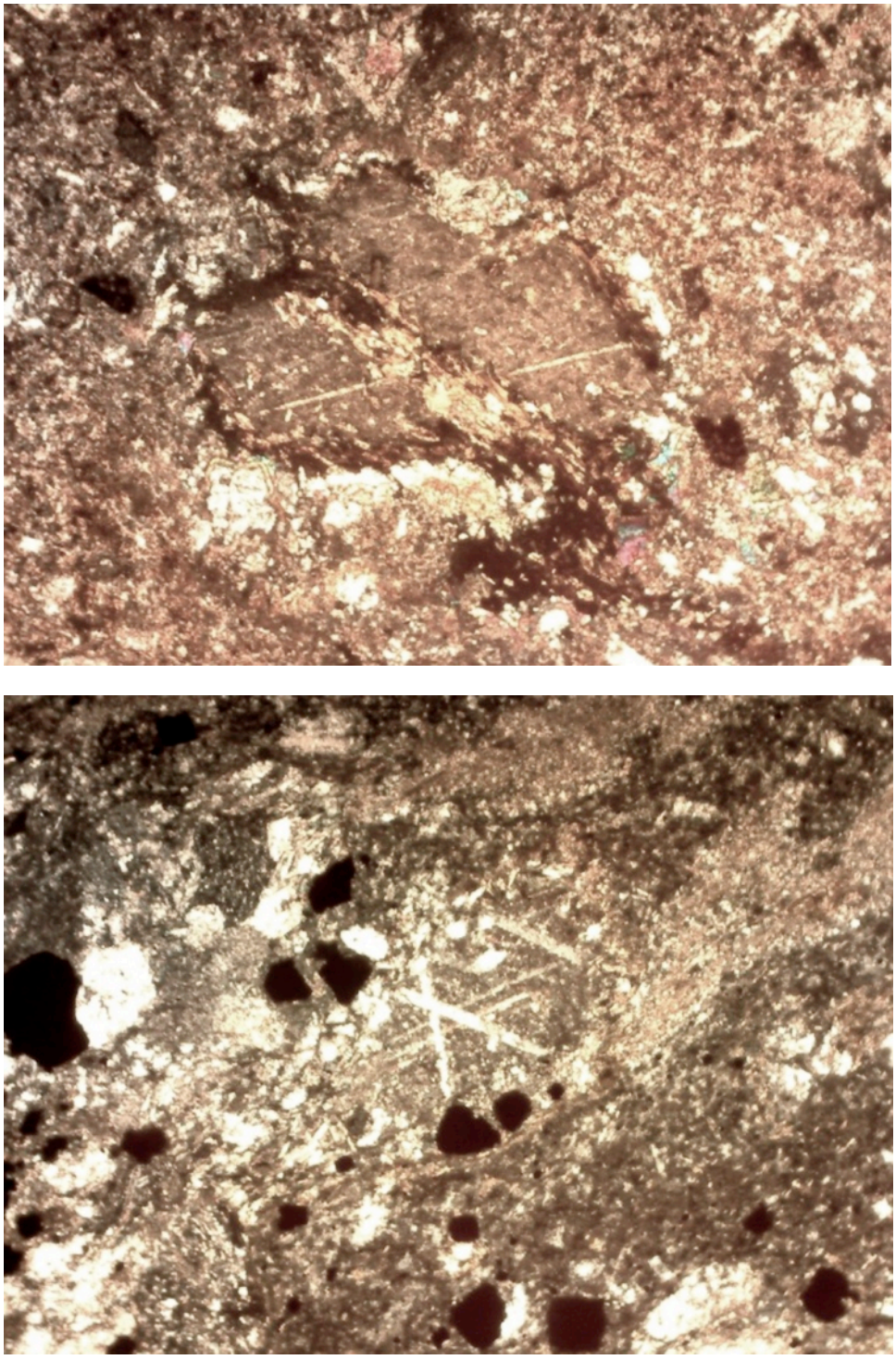

Figure 16. Phenocrysts altering to calcite as seen in the breccia of Frog Lakes clasts. 40x magnification with a field of view approximately 6mm^2.

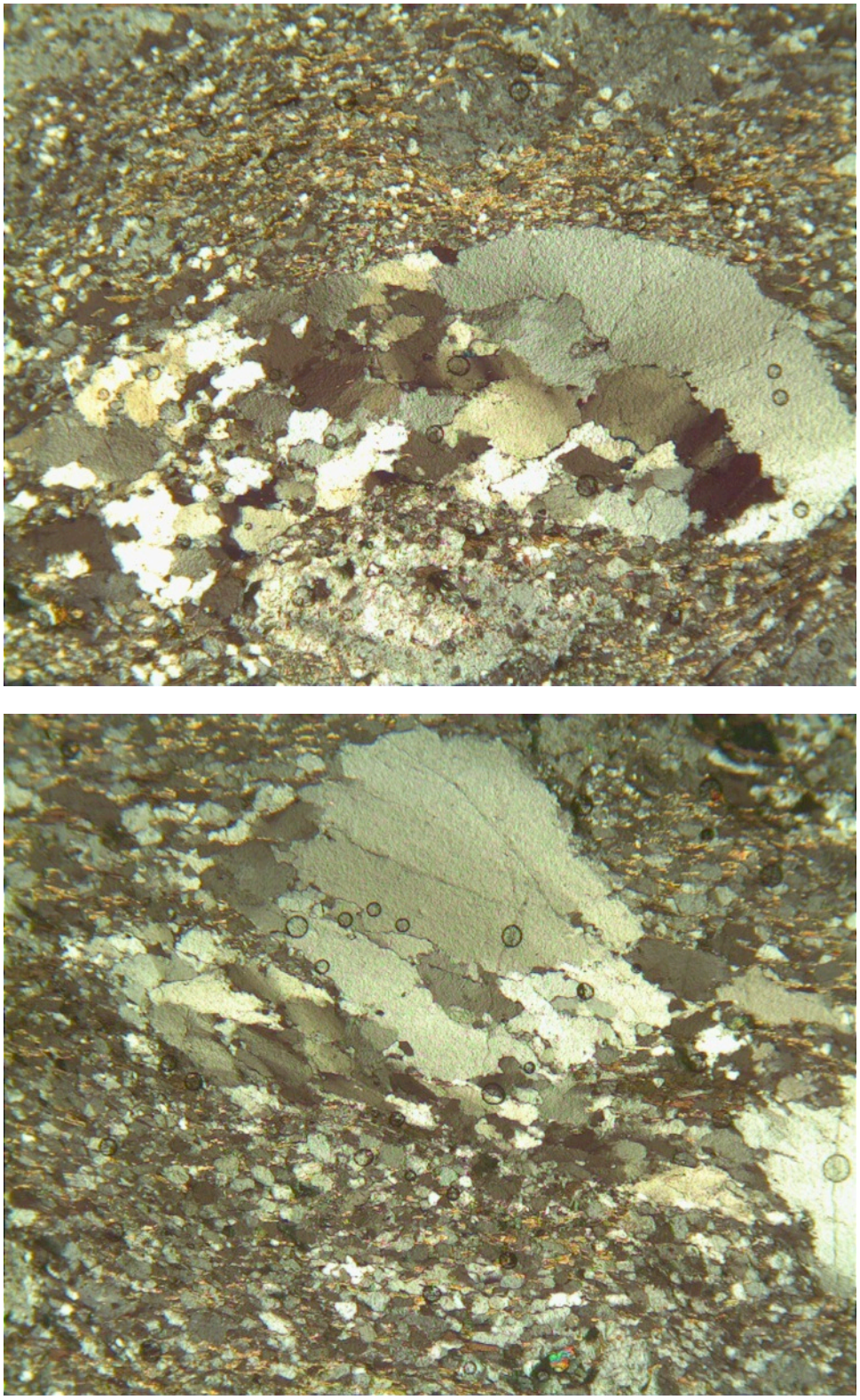

Figure 17. Deformed quartz phenocrysts in the tuff of Greenstone Lake. 40x magnification with a field of view equal to approximately 6mm^2.

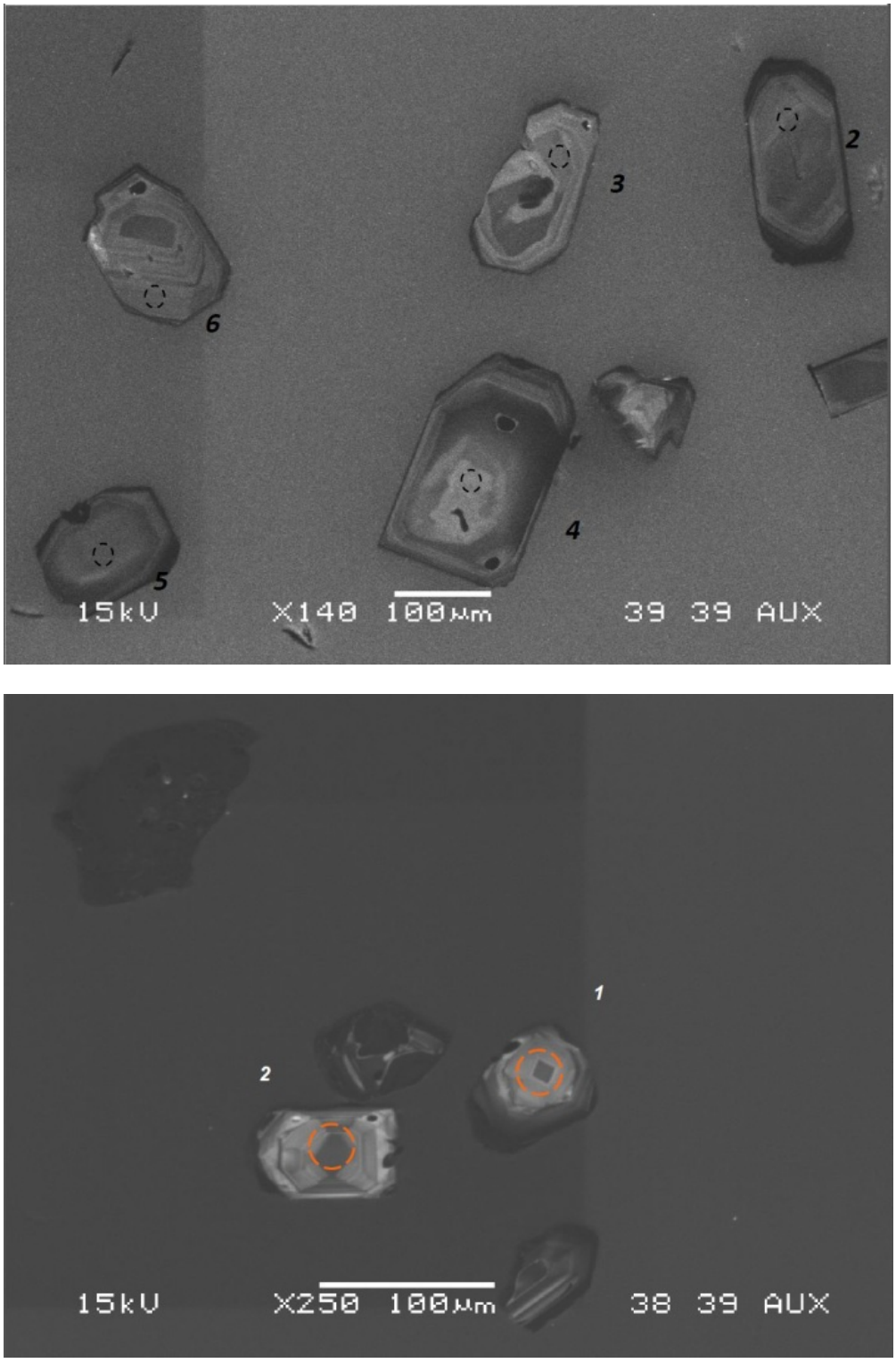

Figure 18. CL images of euhedral to subhedral zircon crystals from the monzodiorite of Saddlebag Lake (upper) and the monzodiorite of Odell Lake (lower). 100 µm bar in each picture for scale. Circle indicates size of primary ion beam relative to zircon crystal.

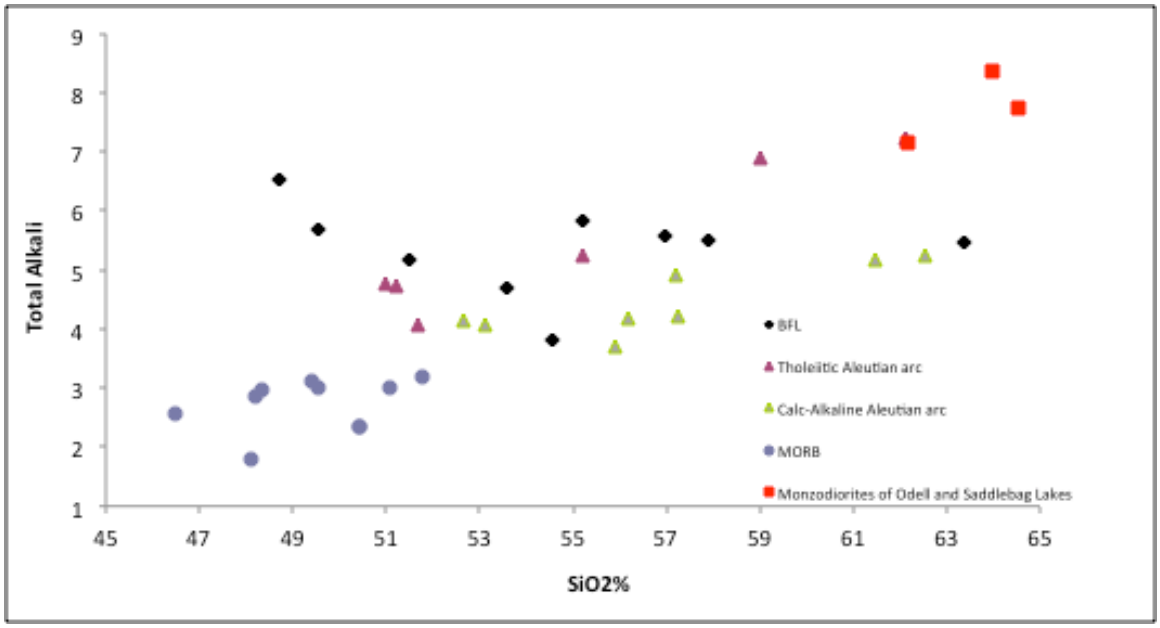

Figure 19. Alkali enrichment in the breccia of Frog Lakes (BFL) clasts is most similar to the tholeiitic Aleutian arc volcanic rocks. Aleutian arc data is from Kay and Kay (1985) and MORB data is from Shibata et al. (1979).

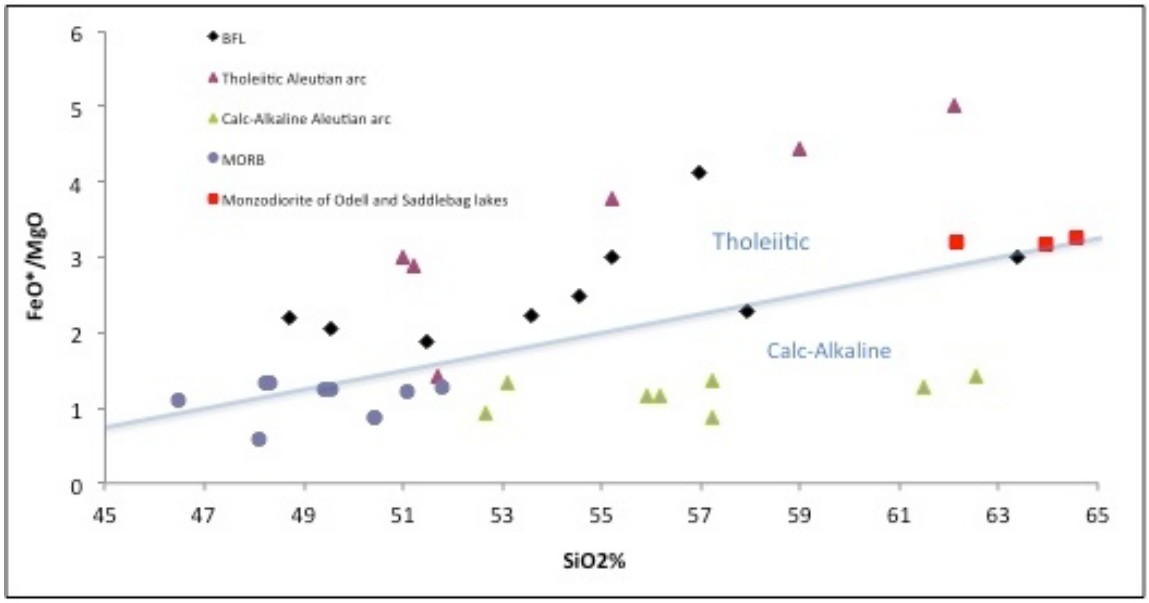

Figure 20. The breccia of Frog Lakes clasts plot with tholeiitic Aleutian arc volcanic rocks in the tholeiitic field in a Miyashiro (1974) diagram. Aleutian arc data is from Kay and Kay (1985) and MORB data is from Shibata et al. (1979).

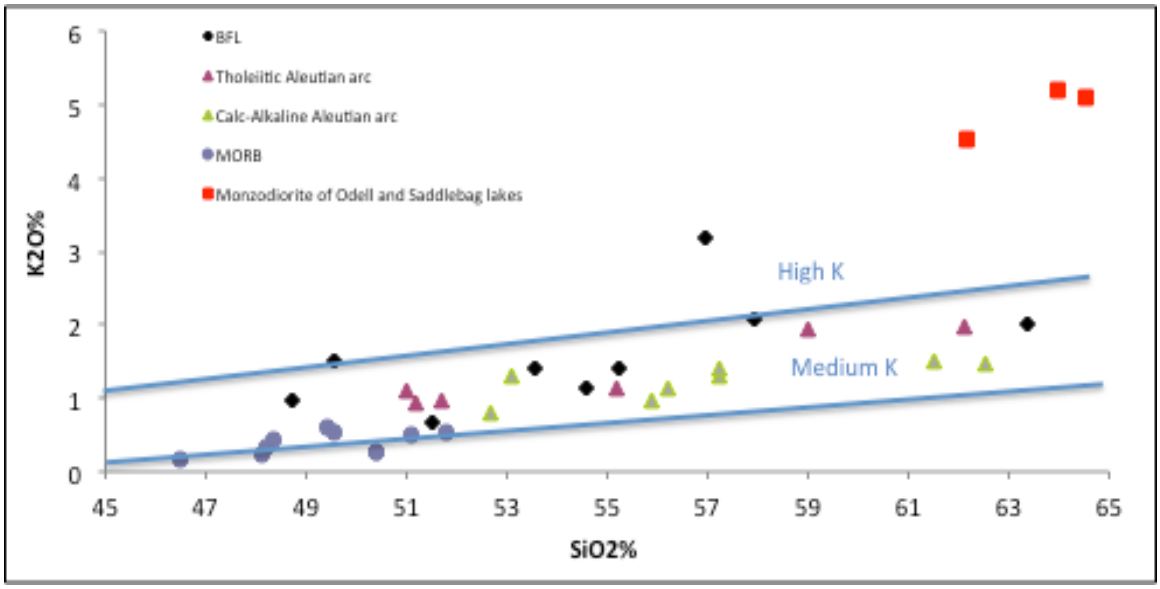

Figure 21. The breccia of Frog Lakes clasts have medium to high K_2O enrichment similar to the volcanic rocks from the Aleutian arc (Gill, 1981). Aleutian arc data is from Kay and Kay (1985) and MORB data is from Shibata et al. (1979).

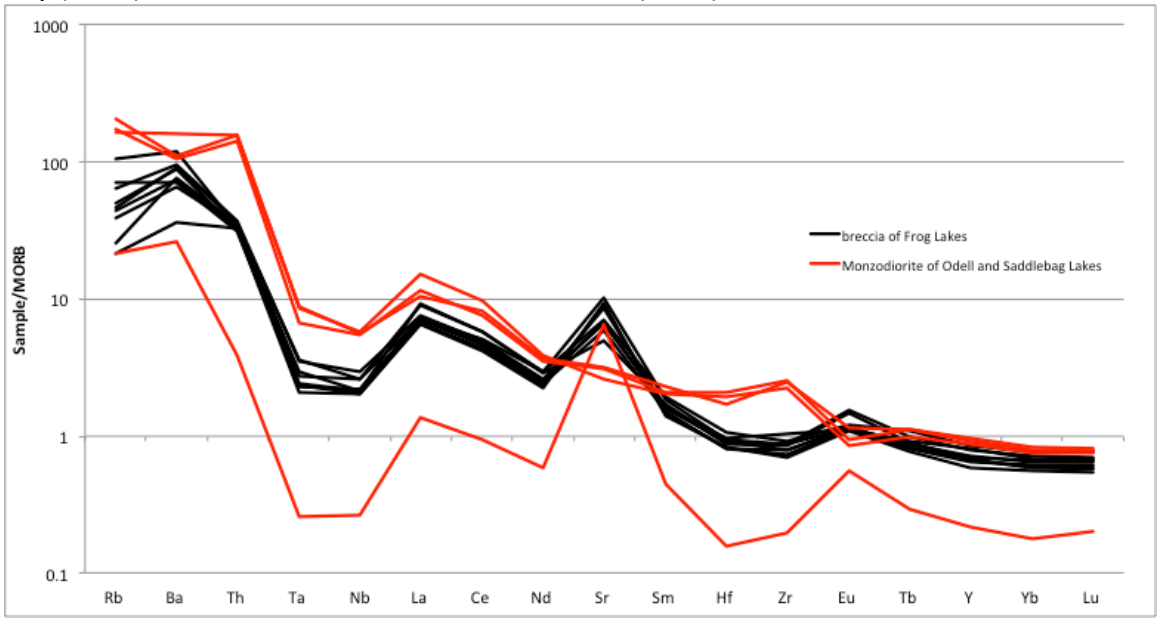

Figure 22. Trace element abundances in breccia of Frog Lakes clasts normalized to MORB (McDonough and Sun, 1995). Enrichment in LILE and depletion in HFSE along with a negative Ta and Nb anomaly are indicative of a magmatic arc petrogenesis.

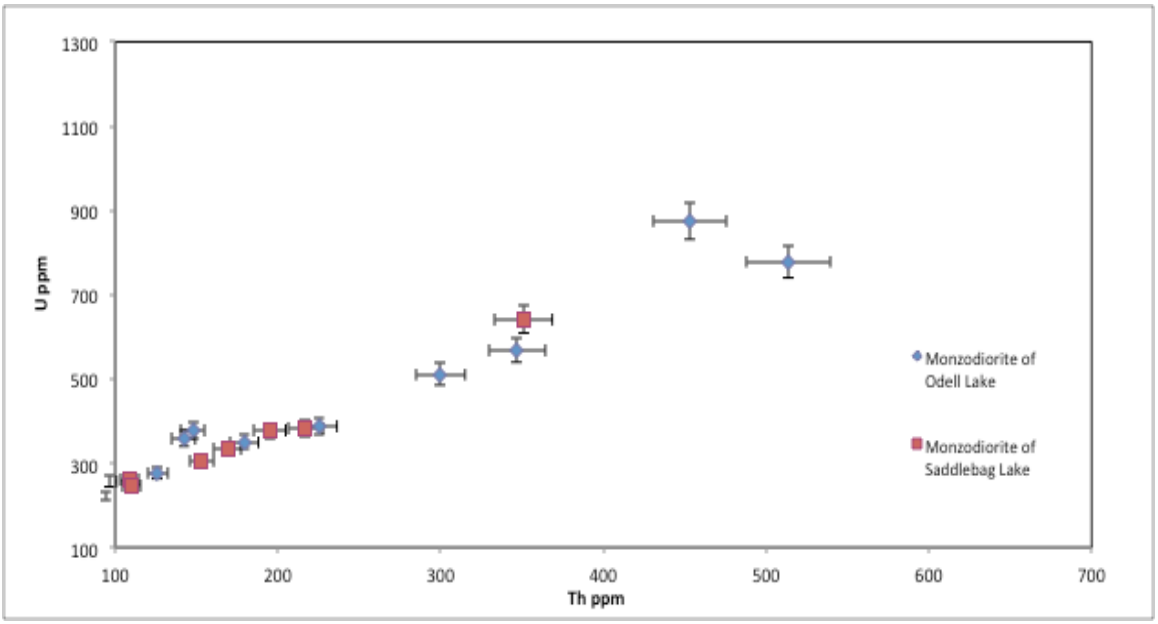

Figure 23. Wide range of U and Th concentrations are seen between the zircons of the monzodiorites of Odell and Saddlebag Lakes.

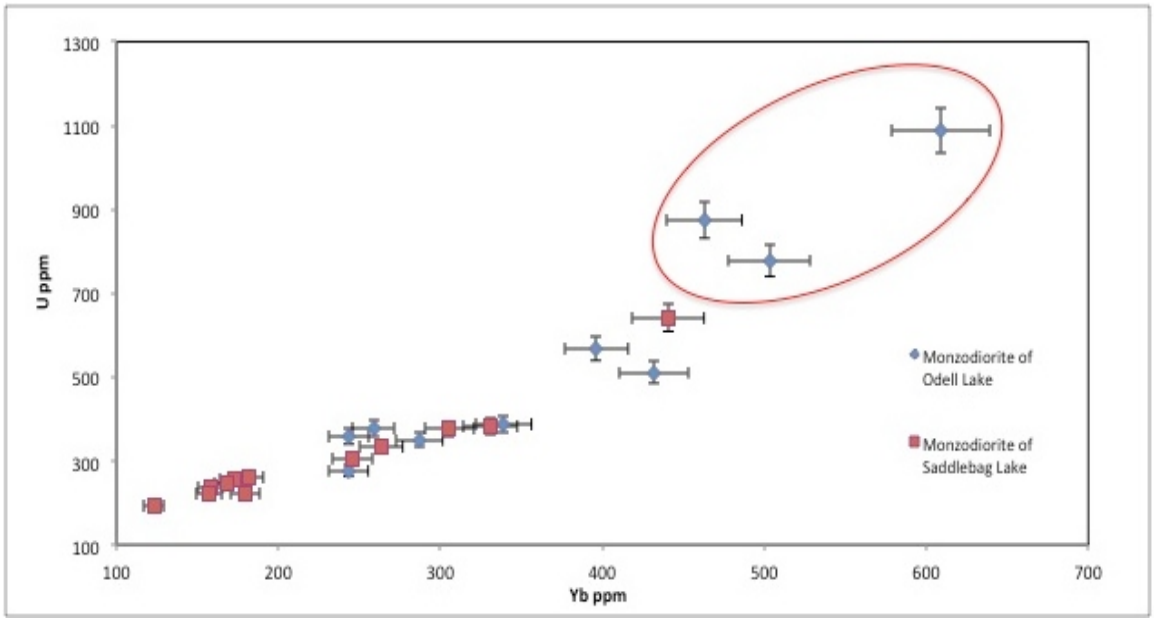

Figure 24. When comparing U versus Yb or any of the lanthanides, a positive correlation of 0.89 is seen in zircons from the monzodiorite of Odell Lake and 0.93 in the zircons from the monzodiorite of Saddlebag Lake. Circled analysis represent the CL-dark rim analysis with the greatest U and Yb concentrations.

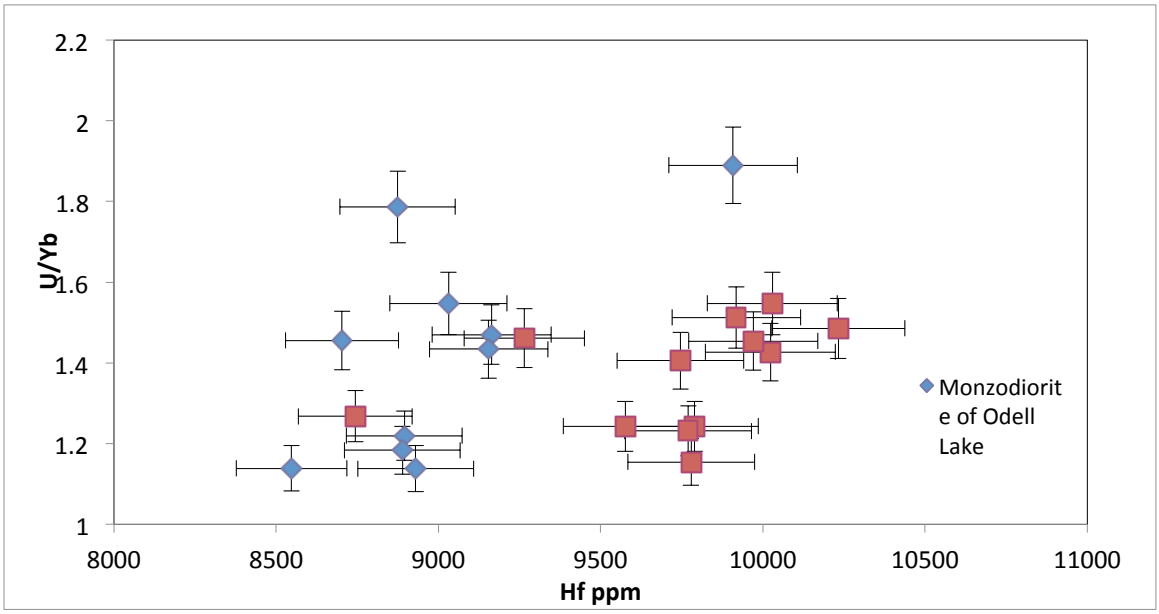

Figure 25. The positive correlation between U and Yb results in a ratio that when plotted against Hf, shows more chemical indistinction between the zircons of the monzodiorites.

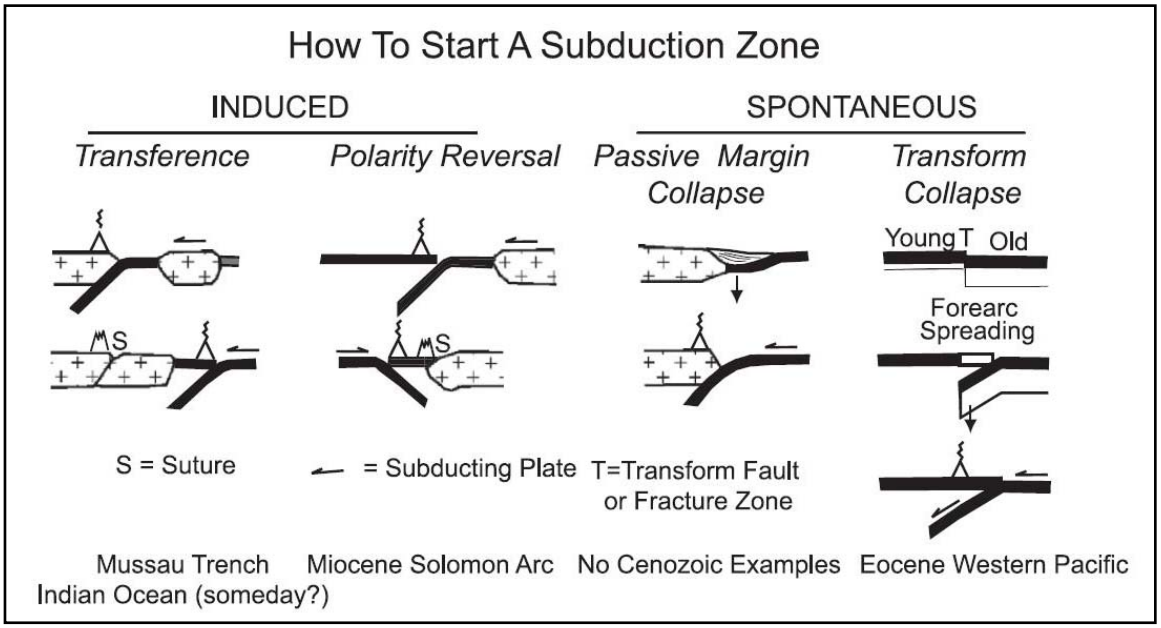

Figure 26. Models of subduction initiation proposed by Stern (2004). Spontaneous nucleation, SNSZ, is shown to the far right.

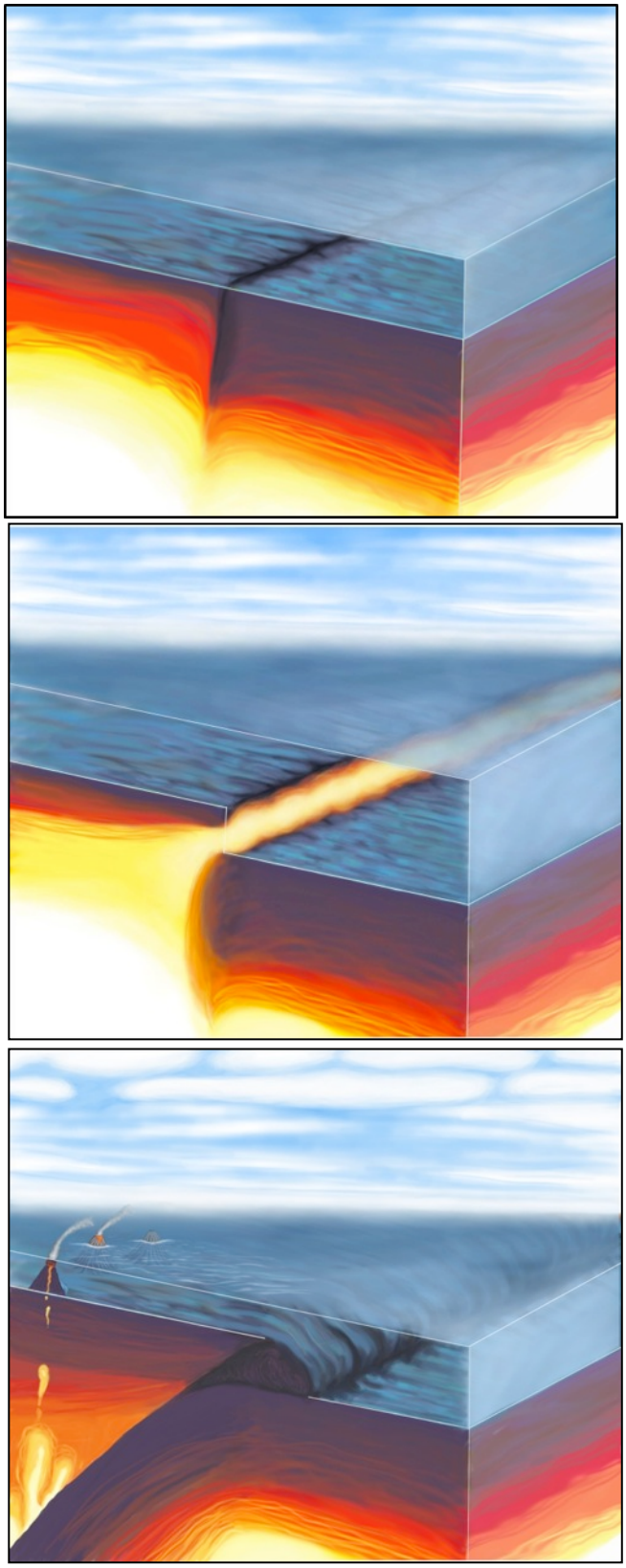

Figure 27. Illustration of subduction initiation by spontaneous nucleation, followed by the production of boninites and the development of an island arc.

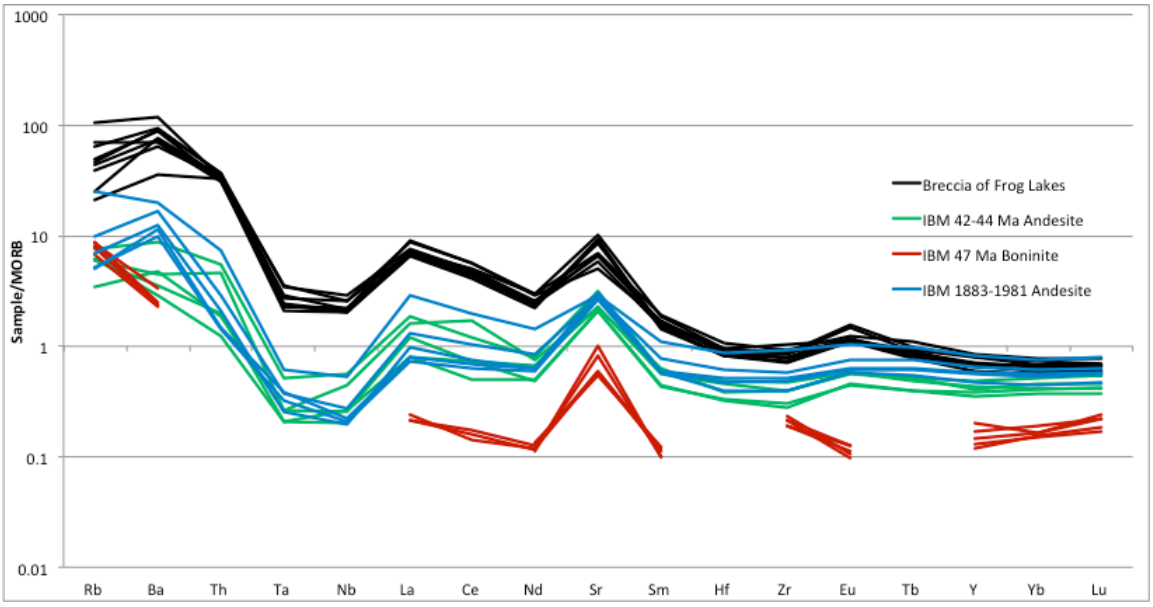

Figure 28. Progressive enrichment in LILE and HFSE as the Izu-Bonin-Mariana (IBM) arc matured from very depleted 47 Ma boninites to 1883-1981 andesite. Data are from Taylor et al. (1993), Ishizuka et al. (2006), and Elliott et al. (1997).

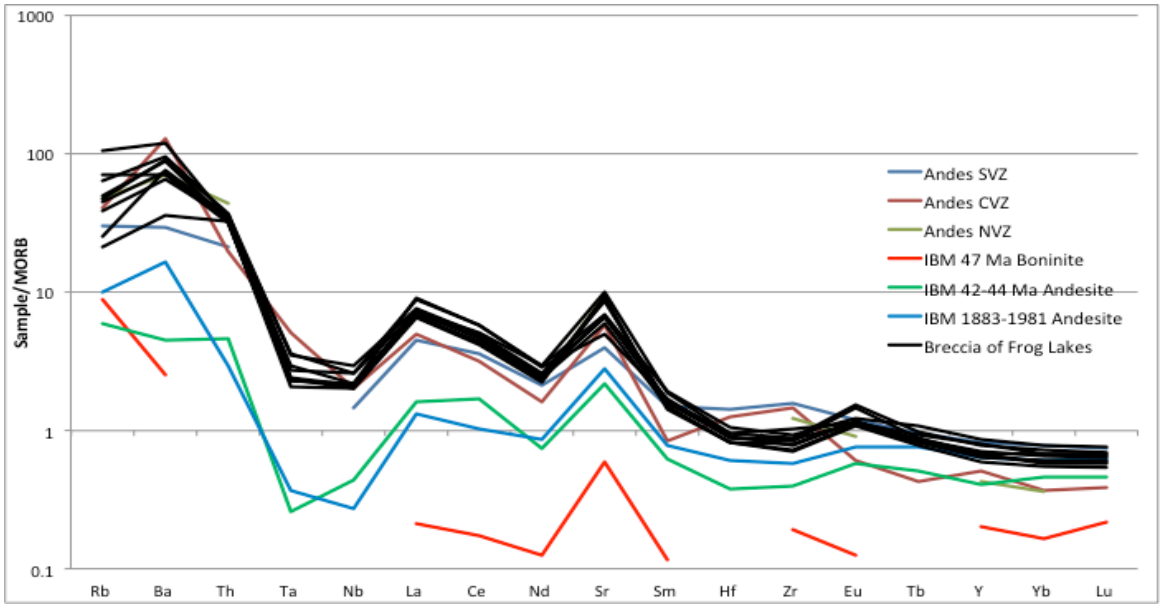

Figure 29. Trace element concentrations of the breccia of Frog Lakes compared to Izu-Bonin-Marianas (IBM) volcanic rocks and andesites from the northern, central, and southern volcanic zones (NVZ, CVZ, and SVZ respectively) of the Andes (Feininger and Seguin, 1983; Hickey-Vargas et al., 1989; Hildreth and Moorbath, 1988; Hora et al., 2007; Mamani et al., 2009; Monzier et al, 1999; Taylor et al., 1993; Ishizuka et al., 2006; Elliott et al., 1997).

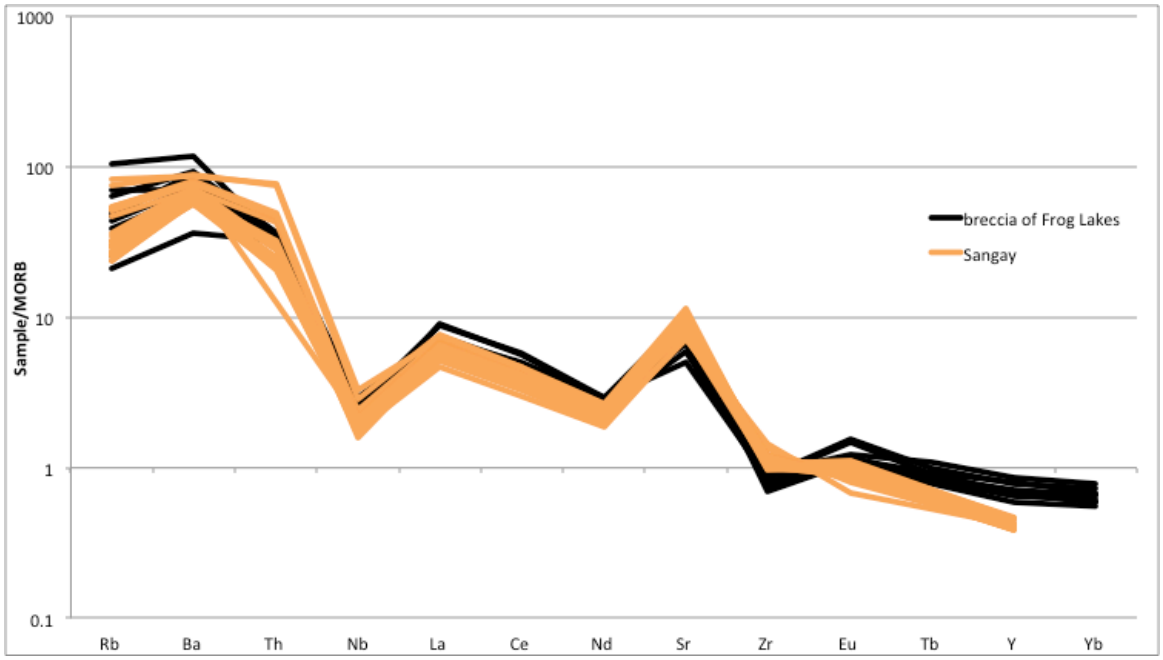

Figure 30. Trace element data from Sangay Volcano in the Northern Volcanic Zone is similarly enriched compared to the breccia of Frog Lakes clasts. Data is from Monzier et al., 1999).

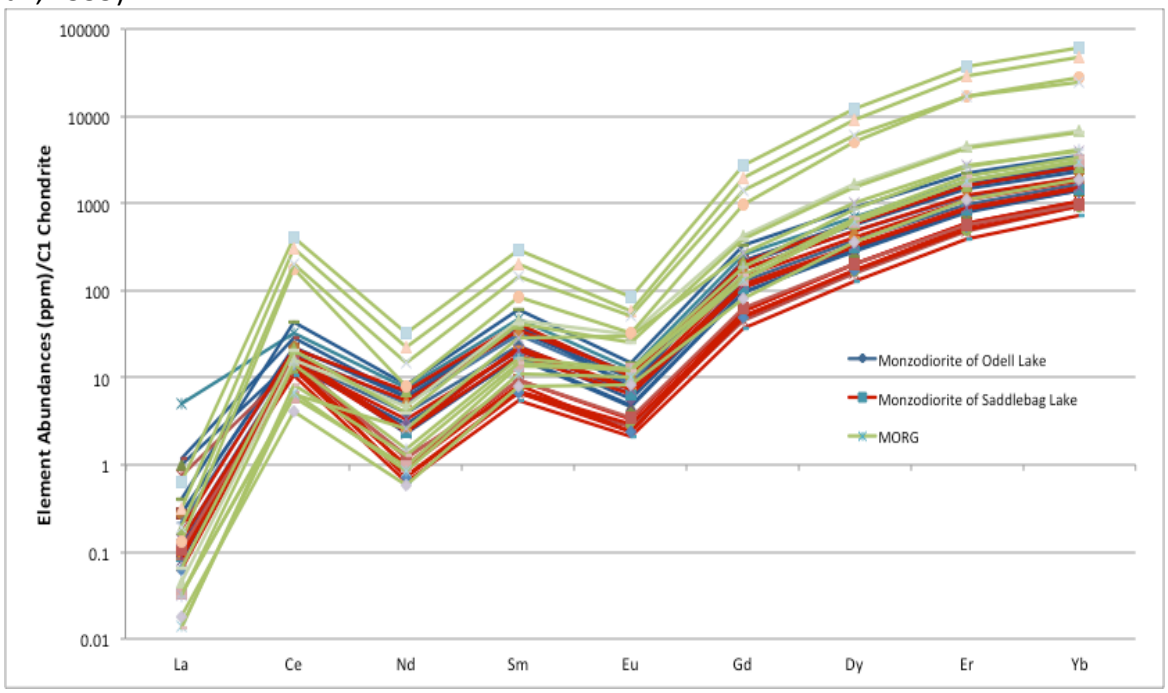

Figure 31. Rare earth element abundances from the monzodiorites and MORG. Discrimination of oceanic or continental origin of each rock type based on enrichments and depletions is impossible due to the overlap in measured trace element abundances. MORG data from Grimes et al., (2007).

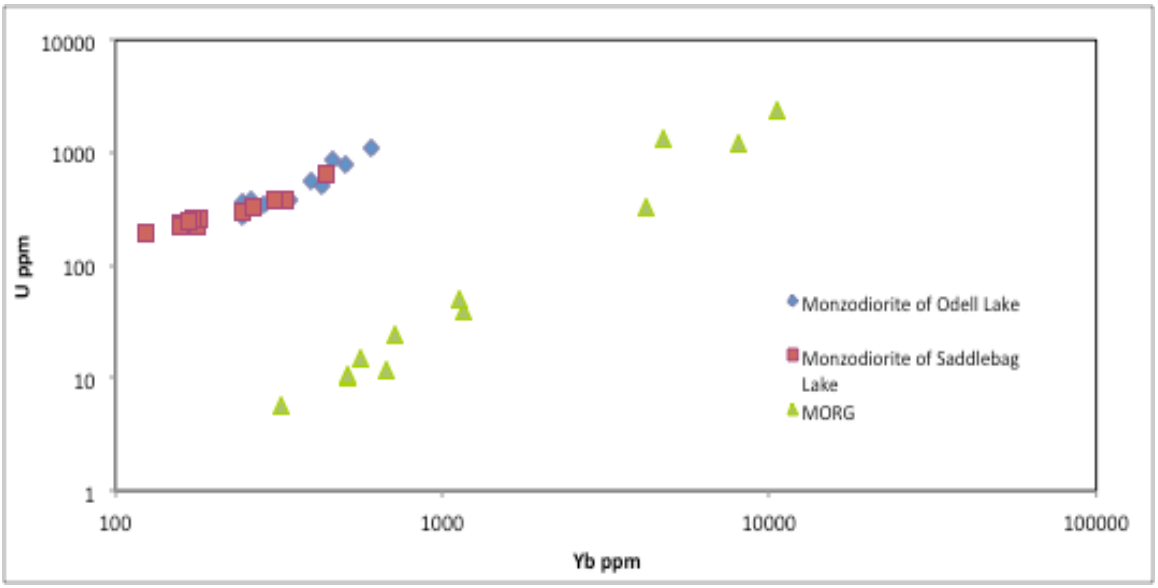

Figure 32. Distinct fields segregating the monzodiorites from MORG are seen when comparing U to Yb. MORG data from Grimes et al. (2007). Error is accounted for with the symbol size.

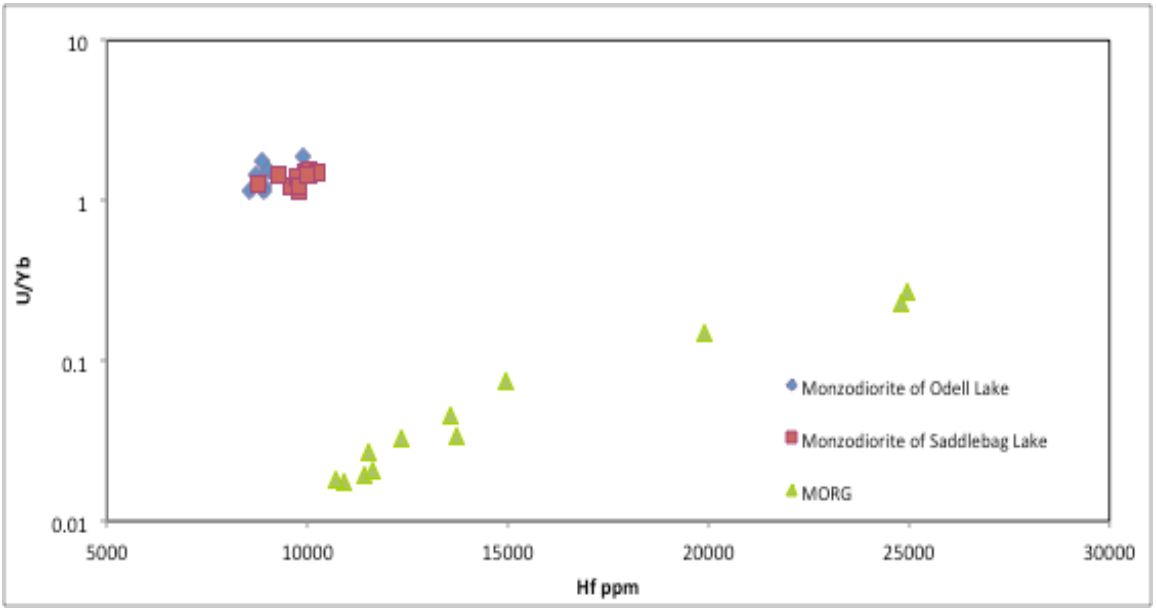

Figure 33. Ratios of fluid mobile elements (such as U) over fluid immobile elements (such as Yb) also discriminate between zircons from magmatic arc and zircons with depleted mantle affinity. MORG data from Grimes et al. (2007).

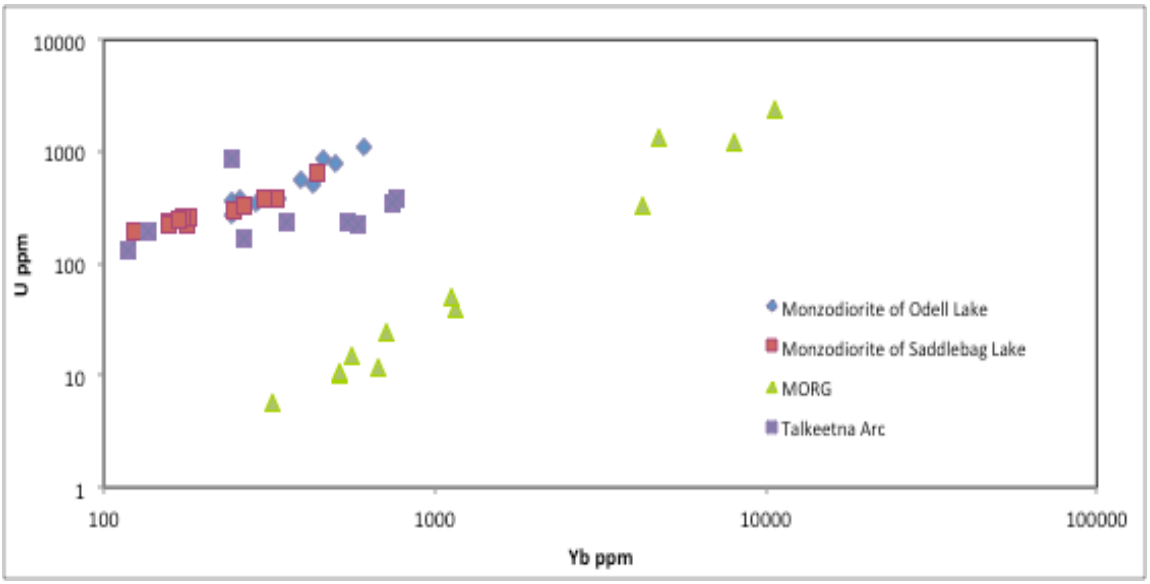

Figure 34. A petrogenetic relationship between the monzodiorites and the Talkeetna arc is shown when comparing fluid mobile versus fluid immobile elements. Talkeetna arc data is from Grimes et al. (2007).

References

Bailey, J.C., 1981, Geochemical criteria for a refined tectonic discrimination of orogenic andesites: Chemical Geology, v.32, p. 139-154.

Barth, A.P., Walker, J.D., Wooden, J.L., Riggs, N.R., and Schweickert, R.A., 2011, Birth of the Sierra Nevada magmatic arc: Early Mesozoic plutonism and volcanism in the east-central Sierra Nevada of California: Geosphere, v. 7, no., 4, p. 877-897.

Bateman, P.C., Kistler, R.W., Peck, D.L., and Busacca, A.J., 1983, Geologic map of the Tuolumne Meadows Quadrangle, Yosemite National Park, California: U.S. Geological Survey Map GQ-1570, scale 1:62,500.

Belousova, E.A., Griffin, W.L., and O'Reilly, S.Y., 2006, Zircon crystal morphology, trace element signatures and Hf isotope composition as a tool for petrogenetic modeling: Examples from eastern Australian granitoids: Journal of Petrology, v. 47, no. 2, p. 329-353.

Bloomer, S.H., and Hawkins, J.W., 1987, Petrology and geochemistry of boninite series volcanic rocks from the Mariana trench: Contributions to Mineralogy and Petrology, v. 97, p. 361-377.

DeBari, S.M. and Sleep, N.H., 1991, High-Mg, low-Al bulk composition of the Talkeetna island arc, Alaska: implications for primary magmas and the nature of arc crust: Geological Society of America Bulletin, v.103, p. 37-47.

Dickinson, W.R., 2000, Geodynamic interpretation of Paleozoic tectonic trends in oriented oblique to the Mesozoic Klamath-Sierran continental margin in California, *in* Soreghan, M.J., and Gehrels, G.E., eds., Paleozoic and Triassic paleogeography and tectonics of western Nevada and northern California: Boulder, Colorado, Geological Society of America Special Paper 347, p. 209-245.

Dickinson, W.R., 2004, Evolution of the North American cordillera: Annual Reviews of Earth and Planetary Sciences, v. 32, p. 13-45.

Douglas, S.R., Riggs, N.R., and Barth, A.P., 2010, The breccia of Frog Lakes: Reconstructing Triassic volcanism in the east-central Sierra Nevada, California: Geological Society of America Abstracts with Programs v. 42, no. 5, p. 296.

Elliott, T.R., Plank, T., Zindler, A., White, W., and Bourdon, B., 1997, Element transport from slab to volcanic front at the Mariana arc: Journal of Geophysical Research, v. 102, p. 14,991-15,019.

Feininger, T., and Seguin, M.K., 1983, Simple Bouguer anomaly field and the inferred crustal structure of continental Ecuador: Geology, v. 11, p. 40-44.

Gill, J.B., 1981, Orogenic andesites and plate tectonics: New York, Springer-Verlag, p. 330.

Greene, D.C., Schweickert, R.A., and Stevens, C.H., 1997, Roberts Mountains allochthon and the western margin of the Cordilleran miogeocline in the northern Ritter Range pendant, eastern Sierra Nevada, California: Geological Society of America Bulletin, v. 109, p. 1294-1305.

Grimes, C.B., John, B.E., Kelemen, P.B., Mazdab, F.K., Wooden, J.L., Cheadle, M.J., Hanghøj, K., and Schwartz, J.J., 2007, Trace element chemistry of zircons from oceanic crust: A method for distinguishing detrital zircon provenance: Geology, v. 35, no. 7, p. 643-646.

Hickey-Vargas, R., Roa, H.M., Escobar, L.L, and Frey, F.A., 1989, Geochemical variations in Andean basaltic and silicic lavas from the Villarrica-Lanin volcanic chain (39.5°S): an evaluation of source heterogeneity, fractional crystallization and crustal assimilation: Contribution to Mineralogy and Petrology, v. 103, p. 361-386.

Hildreth, W., and Moorbath, S., 1988, Crustal contributions to arc magmatism in the Andes of central Chile: Contribution to Mineralogy and Petrology, v. 98, p. 455-489.

Hora, J.M., Singer, B.S., and Wörner, G., 2007, Volcano evolution and eruptive flux on the thick crust of the Andean Central Volcanic Zone: $^{40}Ar/^{39}Ar$ constraints from Volcán Parinacota, Chile: Geological Society of America Bulletin, v. 119, p. 343-362.

Huber, N.K., Bateman, P.C., and Wahrhaftig, C., 1989, Geologic map of Yosemite National Park and vicinity, California: U.S. Geological Survey Map I-1874, scale 1:125,000.

Ireland, T.R., 1995, Ion microprobe mass spectrometry: Techniques and applications in cosmochemistry, geochemistry and geochronology, *in* Hyman, M., and Rowe, M., eds., Advances in Analytical Geochemistry: Greenwich, JAI Press, v. 2, p. 1-118.

Ishizuka, O., Kimura, J., Li, Y.B., Stern, R.J., Reagan, M.K., Taylor, R.N., Ohara, Y., Bloomer, S.H., Ishii, T., Hargrove III, U.S., and Haraguchi, S., 2006, Early stages in the evolution of Izu-Bonin arc volcanism: New age, chemical, and isotopic constraints: Earth and Planetary Science Letters, v. 250, p. 385-401.

Kay, S.M., and Kay, R.W., 1985, Aleutian tholeiitic and calc-alkaline magma series I: The mafic phenocrysts: Contribution to Mineralogy and Petrology, v. 90, p. 276-290.

Kelemen, P.B., Hanghøj, K., and Greene, A.R., 2003, One view of geochemistry of subduction-related magmatic arcs, with an emphasis on primitive andesite and lower crust, in Rudnick, R.L., ed., The Crust: Oxford, Elsevier-Pergamon, Treatise on Geochemistry, v. 3, p. 593-650.

Koenig, J.B., 1963, Geologic map of California: Walker Lake sheet: California Division of Mines and Geology, scale 1:250000.

Le Bas, M.J., Le Maitre, R.W., Streckeisen, A., and Zanettin, B., 1986, A chemical classification of volcanic rocks based on the total alkali-silica diagram: Journal of Petrology, v. 27, p. 745-750.

Mamani, M., Wörner, G., and Sempere, T., 2009, Geochemical variations in igneous rocks of the Central Andean orocline (13°S): Tracing crustal thickening and magma generation through time and space: Geological Society of America Bulletin, v. 122, p. 162-182.

McDonough, W.F., and Sun, S.-S., 1995, The composition of the Earth: Chemical Geology, v. 120, p. 223-253.

Miller, E.L., Miller, M.M., Stevens, C.H., Wright, J.E., and Madrid, R., 1992, Late Paleozoic paleogeographic and tectonic evolution of the western U.S. Cordillera, *in* Burchfiel, B. C., Lipman, P.W., and Zoback, M.L., eds., The Cordilleran orogen: Conterminous U.S.: Boulder, Colorado, Geological Society of America, The Geology of North America, v. G-3.

Miyashiro, A., 1974, Volcanic rock series in island arcs and active continental margins: American Journal of Science, v. 274, p. 321-355.

Monzier, M., Robin, C., Samaniego, P., Hall, M.L., Cotton, J., Mothes, P., and Arnaud, N., 1999, Sangay Volcano, Ecuador: structural development, present activity and petrology: Journal of Volcanology and Geothermal Research, v. 90, p. 49-79.

Nilsen, T.H., and Stewart, J.H., 1980, The Antler orogeny-mid-Paleozoic tectonism in western North America: Geology, v. 8, p. 298-302.

Reagan, M.K., Hanan, B.B., Heizler, M.T., Hartman, B.S., and Hickey-Vargas, R., 2008, Petrogenesis of volcanic rocks from Saipan and Rota, Mariana Islands, and implications for the evolution of nascent island arcs: Journal of Petrology, v. 49, p. 441-464.

Saleeby, J., 2011, Geochemical mapping of the Kings-Kaweah ophiolites belt, California-Evidence for progressive mélange formation in a large offset transform-subduction initiation environment, *in* Wakabayashi, J., and Dilek, Y., eds., Mélanges: Processes of Formation and Societal Significance: Boulder, Colorado, Geological Society of America Special Paper 480, p. 31-73.

Schweickert, R.A., and Cowan, D.S., 1975. Early Mesozoic tectonic evolution of the western Sierra Nevada, California: Geological Society of America Bulletin, v. 86, p. 1329-1336.

Schweickert, R.A., and Lahren, M.M., 1987, Continuation of Antler and Sonoma orogenic belts to the eastern Sierra Nevada, California, and late Triassic thrusting in a compressional arc: Geology, v. 15, p. 270-273.

Schweickert, R.A., and Lahren, M.M., 1999, Triassic caldera at Tioga Pass, Yosemite National Park, California: Structural relationships and significance: Geological Society of America Bulletin, v. 111, p. 1714-1722.

Schweickert, R.A., and Lahren, M.M., 2006, Geologic evolution of Saddlebag Lake pendant, eastern Sierra Nevada, California: Tectonic implications, *in* Girty, G., and Cooper, J.D., eds., Using Stratigraphy, Sedimentology, and Geochemistry to Unravel

the Geologic History of the Southwestern Cordillera: Pacific Section, SEPM (Society for Sedimentary Geology), p. 27-56.

Shibata, T., Thompson, G., and Frey, F.A., 1979, Tholeiitic and alkali basalts from the mid-Atlantic ridge at 43° N: Contributions to Mineralogy and Petrology, v. 70, p. 127-141.

Shiraki, K., Kuroda, N., Maruyama, S., and Urano, H., 1978, Evolution of the Tertiary volcanic rocks in the Izu-Mariana Arc: Bulletin of Volcanology, v. 41-4, p. 548-562.

Sorenson, S.S., Dunne, G.C., Hanson, R.B., Barton, M.D., Becker, J. Tobisch, O.T., and Fiske, R.S., 1998, From Jurassic shores to Cretaceous plutons: geochemical evidence for paleoalteration environments of metavolcanic rocks, eastern California: Geological Society of America Bulletin, v. 110, p. 326-343.

Stern, R.J., 2004, Subduction initiation: Spontaneous and induced: Earth and Planetary Science Letters, v. 226, p. 275-292.

Stern, R.J., and Bloomer, S.H., 1992, Subduction zone infancy: Examples from the Miocene Izu-Bonin-Mariana and Jurassic California arcs: Geological Society of America Bulletin, v. 104, p. 1621-1636.

Stone, P., and Stevens, C.H., 1988, Pennsylvanian and early Permian paleogeography of east-central California: Implications for the shape of the continental margin and the timing of continental truncation: Geology, v. 16, p. 330-333.

Strand, R.G., 1967, Geologic map of California: Mariposa sheet: California Division of Mines and Geology, scale 1:250000.

Taylor, R.N., Nesbitt, R.W., Vidal, P., Harmon, R.S., Auvray, B., and Croudace, I.W., 1993, Mineralogy, chemistry, and genesis of the boninites series volcanics, Chichijima, Bonin Islands, Japan: Journal of Petrology, v. 35, p. 577-617.

CURRICULUM VITAE

Sarah Elizabeth Roberts

Education

Ph.D., Earth Sciences, University of Notre Dame, Notre Dame, IN, 2012 to Present

- Lunar Petrology

M.S., Earth Sciences, Indiana University-Purdue University Indianapolis, Indianapolis, IN 2013

- Thesis: Breccia of Frog Lakes: Reconstructing Triassic volcanism and subduction initiation in the east-central Sierra Nevada, California

M.A., Painting, University of Alabama, Tuscaloosa, AL, 2005

- Thesis: My Backyard

B.F.A., Painting, Birmingham-Southern College, Birmingham, AL, 2003

Publications

Barth, A.P., Feilen, A.D.G., Yager, S.L., Douglas, S.R., Wooden, J.L., Riggs, N.R., and Walker, J.D., 2012, Petrogenetic connections between ash-flow tuffs and granodioritic to granitic intrusive suite in the Sierra Nevada arc, California: Geosphere 8, 250-264, doi: 10.1130/GES000737.1.

Conference Presentations

2013. Roberts, S.E., Neal, C.R. Petrography is still relevant! Examination of lunar melt rocks to determine formation and evolution. 44th Lunar and Planetary Science Conference. (poster)

Yager, S., Barth, A.P., Douglas, S.R., Walker, J.D., Riggs, N.R., and Schweickert, R.A., 2012, Magmatic compositions and alteration of rhyolitic ash-flow tuffs in the eastern Sierran arc of California: Geological Society of America Abstracts with Programs v. 44, no. 7, p. 244.

2011. Douglas, S.R., Riggs, N.R., Barth, A.P., and Economos, R.C. The Breccia of Frog Lakes: Record of Mafic Arc Magmatism in the Mesozoic Sierra Nevada, California. American Geophysical Union Fall Meeting, San Francisco, California. (poster)

2010. Douglas, S.R., Riggs, N.R., Barth, A.P., and Walker, J.D. Breccia of Frog Lakes: Reconstructing Triassic volcanism in the east-central Sierra Nevada, California. Geological Society of America National Meeting, Denver, Colorado. (poster)

Research Experience

M.S. Thesis Research

Petrology lab, Indiana University-Purdue University Indianapolis, Indianapolis, IN 2010-2012

- Preparation of rock samples for geochemical analysis and thin section preparation.

Stanford University, Stanford, California, 2011

- Mineral Separation and Scanning Electron Microscopy.

Undergraduate Research

Petrology lab, Indiana University-Purdue University Indianapolis, Indianapolis, IN, 2009-2010

- Preparation of rock samples for geochemical analysis and thin section preparation.

Short Courses

SIMS workshop, University of California in Los Angeles, February 2011

- Week long workshop funded by the National Science Foundation.

Teaching Experience

Graduate Teaching Assistant, University of Notre Dame, 2012 to present.

- Assisted professors in grading and labs.

Graduate Teaching Assistant, Indiana University-Purdue University Indianapolis, 2010-1012.

- Introduction physical geology lab.
- Responsible for creating all class material including syllabi, labs, quizzes, and exams.
- Taught 9 classes and 162 students over 4 semesters.

Field Experience

Field Camp, Indiana University Judson Mead Field Station, Montana, 2011

- Mapping, lithologic descriptions, brunton, and GPS use.

Field Work, Inyo National Forest and Sequoia National Forest, California, 2011

- Mapping, photography, and lithologic descriptions.

Field Work, Joshua Tree National Park, California, 2010

- Mapping, lithologic descriptions, brunton and GPS use.